Toward Accessible Biophotonics

Instrumentation for Insect and Vegetation Applications

Månefjord, Hampus

2024

Document Version:
Publisher's PDF, also known as Version of record

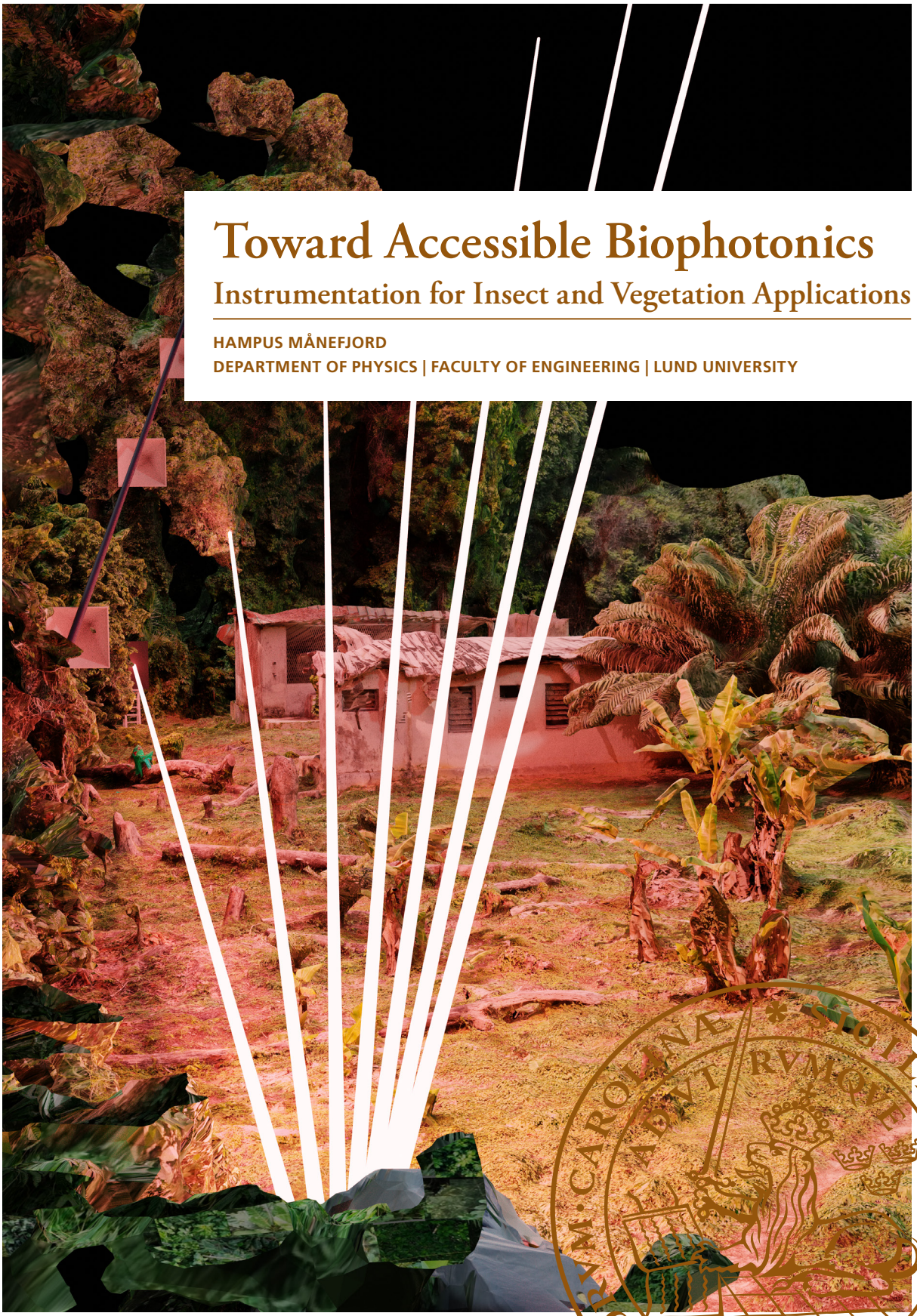

Toward Accessible Biophotonics

Instrumentation for Insect and Vegetation Applications

HAMPUS MÅNEFJORD
DEPARTMENT OF PHYSICS | FACULTY OF ENGINEERING | LUND UNIVERSITY

Toward Accessible Biophotonics

Instrumentation for Insect and Vegetation Applications

Hampus Månefjord

LUND
UNIVERSITY

DOCTORAL DISSERTATION

Doctoral dissertation for the degree of Doctor of Philosophy (PhD) at the Faculty of Engineering at Lund University to be publicly defended on 24th of May 2024 at 13.15 in the Rydberg hall, Department of Physics, Professorsgatan 1, Lund.

Faculty opponent

Pablo Loza-Alvarez

Organization: LUND UNIVERSITY

Document name: DOCTORAL DISSERTATION **Date of issue:** 2024-05-24

Author: Hampus Månefjord **Sponsoring organization:**

Title and subtitle: Toward Accessible Biophotonics

Instrumentation for Insect and Vegetation Applications

Abstract: Biophotonics instrumentation for studying insects and vegetation is crucial to prevent diseases, improve crops, and understand the ecosystems we live in. However, access to sophisticated scientific equipment remains a barrier in many research settings. To address this, accessible instrumentation is essential for better understanding of biodiversity, plant health, and pest management.

This thesis focuses on the development and implementation of accessible biophotonic instruments for insect and vegetation studies. These include a novel six-dimensional camera that captures spatial, spectral, polarimetric, and goniometric information. This instrument analyzed malaria and Zika mosquito species, sex, age, and gravidity. Additionally, two hyperspectral lidars were created – one for fluorescence, enabling studies of chlorophyll response and monitoring tagged insects (e.g., stingless bees), and the other for elastic light, used for the first-ever remote wing thickness measurements of flying insects. Both lidars are unique in featuring 70 spectral bands.

Accessibility was a core design principle, achieved through open-source designs, low-cost components, 3D printing, modularity, and field readiness. This approach was demonstrated by instrument replication at workshops and deployment at remote sites. This work demonstrates accessible scientific tools with the hope to expand research capabilities and biophotonic discoveries across the globe.

Keywords: Remote sensing, Laser-Induced Fluorescence, Hyperspectral Scheimpflug Lidar, Raytracing, Low-Cost, 3D printing, Entomology, Stingless bees

Classification system and/or index terms (if any): **Supplementary bibliographical information:**

Language: English

ISBN: 978-91-8104-045-6 (print) and 978-91-8104-044-9 (pdf)

Recipient's notes: **Number of pages**: 248

Toward Accessible Biophotonics

Instrumentation for Insect and Vegetation Applications

Hampus Månefjord

LUND
UNIVERSITY

The front cover illustration is a 3D rendering based on drone photos of an experiment site in the Taï rainforest in Côte d'Ivoire. Photos and 3D modelling by Hampus Månefjord.

The back cover is an assembly of photographs by Hampus Månefjord, Josefin Månefjord, Meng Li, Lauro Müller, and Mikkel Brydegaard.

This thesis work was financially supported by the Swedish Research Council through a Uforsk grant with project number 2018-04073. It was also supported by the Swedish International Development Agency (SIDA) through the International Science Program (ISP, Uppsala) by a grant to the African Spectral Imaging Network (AFSIN). Further, by the Royal Physiographic Society in Lund, and the European Research Council (ERC) under the European Union's Horizon 2020 research and innovation program (grant agreement No. 850463).

Faculty of Engineering, Department of Physics

ISBN: 978-91-8104-045-6 (print)
ISBN: 978-91-8104-044-9 (pdf)
LRCP: 254
ISSN: 1102-8718
ISRN: LUTFD2/TCFP-254-SE

Printed in Sweden by Media-Tryck, Lund University
Lund 2024

Media-Tryck is a Nordic Swan Ecolabel certified provider of printed material. Read more about our environmental work at www.mediatryck.lu.se

MADE IN SWEDEN

"*What is an ocean but a multitude of drops*".

- David Mitchell (Cloud Atlas, 2004)

Table of Contents

Abstract

Biophotonics instrumentation for studying insects and vegetation is crucial to prevent diseases, improve crops, and understand the ecosystems we live in. However, access to sophisticated scientific equipment remains a barrier in many research settings. To address this, accessible instrumentation is essential for better understanding of biodiversity, plant health, and pest management.

This thesis focuses on the development and implementation of accessible biophotonic instruments for insect and vegetation studies. These include a novel six-dimensional camera that captures spatial, spectral, polarimetric, and goniometric information. This instrument analyzed malaria and Zika mosquito species, sex, age, and gravidity. Additionally, two hyperspectral lidars were created – one for fluorescence, enabling studies of chlorophyll response and monitoring tagged insects (e.g., stingless bees), and the other for elastic light, used for the first-ever remote wing thickness measurements of flying insects. Both lidars are unique in featuring 70 spectral bands.

Accessibility was a core design principle, achieved through open-source designs, low-cost components, 3D printing, modularity, and field readiness. This approach was demonstrated by instrument replication at workshops and deployment at remote sites. This work demonstrates accessible scientific tools with the hope to expand research capabilities and biophotonic discoveries across the globe.

Populärvetenskaplig sammanfattning

Människors nyfikenhet och drivkraft att förstå och mäta vår värld har lett till många vetenskapliga framsteg. Vårt ständiga sökande efter kunskap har hjälpt oss att bland annat förhindra sjukdomar, förbättra skördar och förstå de ekosystem vi lever i. Dock varierar förutsättningar och utmaningar för forskning runt om i världen, och i många forskningsmiljöer saknas det tillgång till avancerad laboratorieutrustning. För att jämna ut spelplanen är tillgång till lättillgänglig forskningsutrustning en nödvändighet. Därför har jag i detta forskningsprojekt utvecklat två optiska mätinstrument med hjälp av kostnadseffektiva material och komponenter. Instrumenten kan samla in information som är otillgänglig utan dyr och komplex laboratorieutrustning. De är dessutom enkla att förflytta, replikera och tillverka – och därmed bra anpassade för både fältstudier, utbildning och för användning i mindre bemedlade forskningsmiljöer.

Det första instrumentet, ”BIOSPACE” (Artikel I), är en avancerad kamera där man kan snurra runt på det man ska fotografera. Den mäter också hur ljus absorberas, reflekteras, ändrar polarisation och sprids i olika material, som exempelvis insektsvingar eller löv. Eftersom den kan mäta många fler våglängder än det mänskliga ögat kan uppfatta kan den avslöja olika egenskaper hos materialet och producera bilder som innehåller mycket mer information än ett vanligt fotografi.

Det andra instrumentet, en hyperspektral lidar (Artikel II), kombinerar funktionaliteten hos två optiska instrument – en lidar och en hyperspektral kamera. En lidar mäter avstånd med laserljus och en hyperspektral kamera tar bilder med ett högupplöst spektrum av våglängder. Att kombinera detta i samma instrument gör det möjligt att mäta avståndet till ett objekt och samtidigt analysera det. Den hyperspektrala lidarn gör det möjligt att studera vegetationens egenskaper och insekters aktivitetsmönster med stor detaljrikedom från mer än hundra meters avstånd och utan att störa ekosystemet som studeras – bladen kan sitta kvar på träden och insekterna flyger oskadda genom laserstrålen!

Båda dessa instrument har använts i en rad fältstudier som jag presenterar i den här avhandlingen. I Ghana byggde vi en kopia av lidarn och använde den bland annat för att analysera jordbruksgrödor (Artikel VIII) och registrera aktivitetsmönstret hos gaddlösa bin med hjälp av fluorescerande pulver (Artikel V). I Elfenbenskusten använde vi BIOSPACE för att mäta regnskogslevande insekters optiska egenskaper (Artikel VI). Med BIOSPACE lyckades vi även särskilja mellan olika arter av malariamyggor, avgöra deras kön och ålder samt om de bar på ägg eller inte (Artikel IV). Vi har även mätt de tunnaste insektvingarna som någonsin uppmätts (så vitt vi vet), en mygga med 173 nm tjocka vingar (Artikel IV). Med hjälp av lidarn har vi mätt vingtjocklek på flygande insekter– även det den första mätningen i sitt slag (Artikel III).

Målet med det här projektet har varit att ge forskare tillgång till kraftfulla optiska verktyg, oavsett budget och var i världen de befinner sig. Instrumenten är designade med billiga och lättillgängliga komponenter – BIOSPACE är byggd med hjälp av både 3D-printade delar och tekniklego! Ritningar och mjukvara är fritt tillgängliga för att uppmuntra alla intresserade att kopiera dem till sin forskning eller utbildningsverksamhet. Förhoppningen är att dessa verktyg kommer att främja ett mer jämlikt forskningslandskap och möjliggöra nya biologiska upptäckter.

Popular science summary

Human curiosity and the drive to understand and measure our world have led to many scientific advances. Our constant search for knowledge has helped us, among other things, to prevent diseases, improve crops, and understand the ecosystems we live in. However, conditions and challenges for research vary around the world, and many research environments lack access to advanced laboratory equipment. To level the playing field, accessible instrumentation is a necessity. Therefore, I have developed two optical measuring instruments in my research project using cost-effective materials, methods, and components. These instruments can collect information that is inaccessible without expensive and complex laboratory equipment. They are also easy to move, replicate, and manufacture – and thus well adapted for field studies, education, and use in less well-funded research environments.

The first instrument, "BIOSPACE" (Paper I), is an advanced camera that can spin around the target of the photograph. It also measures how light is absorbed, polarized, reflected, and scattered in various materials, such as insect wings, or leaves. Since BIOSPACE can measure many more wavelengths than the human eye can perceive, it can reveal different properties of the material and produce images that contain much more information than a standard photograph.

The second instrument, a hyperspectral lidar (Paper II), combines the functionality of two optical instruments – a lidar and a hyperspectral camera. A lidar measures distances with laser light, and a hyperspectral camera takes pictures with a high-resolution spectrum of wavelengths. Combining this in the same instrument makes it possible to measure the distance to an object and simultaneously analyze it. The hyperspectral lidar enables the study of vegetation properties and insect activity patterns in great detail from over a hundred meters distance without disturbing the ecosystem being studied – the leaves can remain on the trees, and insects can fly through the laser beam unharmed!

Both instruments have been used in a series of studies that I present in this thesis. In Ghana, we built a copy of the lidar and used it to analyze crops (Paper VIII) and to record the activity patterns of stingless bees using fluorescent powder (Paper V). In the Ivory Coast, we used BIOSPACE to measure the optical properties of rainforest-dwelling insects (Paper VI). With BIOSPACE, we were also able to distinguish between different species of malaria mosquitoes, and determine their gender, age, and whether they were carrying eggs or not (Paper IV). We have also measured the thinnest wings ever recorded (to our knowledge), a mosquito with 173 nm thick wings (Paper IV). With the lidar, we have measured wing thickness on flying insects – the first measurement of its kind (Paper III).

The goal of this project has been to give researchers access to powerful optical tools, regardless of budget and where in the world they are located. The instruments are designed with inexpensive and readily available components – BIOSPACE is built with both 3D-printed parts and LEGO Technic! My drawings and software are freely available to encourage anyone interested to copy them for their research or educational activities. Hopefully, these tools will promote a more equitable research landscape and enable new biological discoveries.

Abbreviations

BIOSPACE – Biophotonics, Imaging, Optical, Spectral, Polarimetric, Angular, and Compact Equipment. A multidimensional camera presented in Paper I.

BRDF - Bidirectional Reflectance Distribution Function

CCD – Charge-Coupled Device

CMOS - Complementary Metal-Oxide-Semiconductor

DoLP – Degree of Linear Polarization

EHSL– Elastic HyperSpectral Lidar, presented in Paper III

FHSL – Fluorescence HyperSpectral Lidar, presented in Paper II

FMCW - Frequency Modulated Continuous Wave

FWHM – Full Width at Half Maximum

FWC – Full Well Capacity

HCA - Hierarchical Clustering Analysis

HDR – High Dynamic Range

InGaAs - Indium Gallium Arsenide

LED – Light-Emitting Diode

LD – Laser Diode

Lidar – Light detection and ranging

NIR – Near InfraRed, light with wavelengths from ~700-1000 nm.

PSF – Point Spread Function

Radar – Radio detection and ranging

RGB – Red, Green, and Blue

SIF – Solar-Induced Fluorescence

SNR – Singal-to-Noise Ratio

SVD – Singular Value Decomposition

SWIR – Short Wave InfraRed, light with wavelengths from ~900-1700 nm

ToF – Time of Flight

UV – UltraViolet, light with wavelengths from ~100-400 nm

List of papers

I. **Månefjord, H**., M. Li, C. Brackmann, N. Reistad, A. Runemark, J. Rota, B. Anderson, J. T. Zoueu, A. Merdasa and M. Brydegaard (2022). "*A biophotonic platform for quantitative analysis in the spatial, spectral, polarimetric, and goniometric domains*." Review of Scientific Instruments 93(11).

II. **Månefjord, H**., L. Müller, M. Li, J. Salvador, S. Blomqvist, A. Runemark, C. Kirkeby, R. Ignell, J. Bood and M. Brydegaard (2022). "*3D-Printed Fluorescence Hyperspectral Lidar for Monitoring Tagged Insects*." IEEE Journal of Selected Topics in Quantum Electronics 28(5): 1-9.

III. Müller, L., M. Li, **H. Månefjord**, J. Salvador, N. Reistad, J. Hernandez, C. Kirkeby, A. Runemark and M. Brydegaard (2023). "Remote Nanoscopy with Infrared Elastic Hyperspectral Lidar." Advanced Science 10(15): 2207110.

IV. **Månefjord. H,** M. Li, J. Hernandez, L. Müller, C. Brackman, A. Merdasa, M. D. Bulo, C. Kirkeby, R. Ignell, M. Brydegaard (In preparation). *The deadliest animals with the thinnest wings – near infrared properties of tropical mosquitoes.*

V. **H. Månefjord,** A. A. Huzortey, R. Boateng, Y. A. Gbogbo, A. S. D. Yamoa, J. T. Zoueu, P. K. Kwapong, B. Anderson, M. Brydegaard (In review). *"Hyperspectral Lidar for Monitoring High-resolution Activity Patterns of African Stingless Bee Species.*

VI. **H. Månefjord,** A. S. D. Yamoa, Y. A. Gbogbo, L. Müller, A. Runemark, B. K. Kouakou, R. Boateng, A. A. Huzortey, I. K. Badu, M. Brydegaard, J. T. Zoueu, B. Anderson, M. Li (In preparation). *"Insect Stratification and Diversity Across Taï Virgin Forest Canopy, Côte d'Ivoire – With Entomological Lidar"*

VII. **H. Månefjord,** M. Li, J. Salvador, A. Runemark, C. Kirkeby, and M. Brydegaard (2022). "*Low-Cost and Lightweight Hyperspectral Lidar for Mapping Vegetation Fluorescence.*" EPJ Web of Conferences ILRC Proceedings**:** 213-218

VIII. R. Boateng, A. A. Huzortey, Y. A. Gbogbo, J. T. Zoueu, M. Brydegaard, B. Anderson and **H. Månefjord** (2023). "*Remote Vegetation Diagnostics in Ghana with a Hyperspectral Fluorescence Lidar.*" IEEE Journal of Selected Topics in Quantum Electronics 29(4: Biophotonics): 1-7

IX. R. Boateng, A. A. Huzortey, A. Y. Gbogbo, D. A. Yamoa, J. T. Zoueu, M. Brydegaard, **H. Månefjord** and B. Anderson (2023). "*Mapping of Algae on Walls with a 3D Printed Hyperspectral Fluorescence Lidar.*" Laser Science, Optica Publishing Group: JM7A 76

X. **H. Månefjord,** M. Li, C. Brackmann, N. Reistad, A. Merdasa and M. Brydegaard (2021). *"BIOSPACE–A low-cost platform for problem-based learning in Biophotonics"* 2021: Conference on Teaching and Learning -Proceedings 11.

XI. M. Brydegaard, R. D. Pedales, V. Feng, A. S. D. Yamoa, B. Kouakou, **H. Månefjord,** L. Wührl, C. Pylatiuk, D S. Amorim, R. Meier (Accepted, 2024) "*Towards global insect biomonitoring with frugal methods"* Philosophical Transactions of the Royal Society B

Related work

XII. H. Chen, M. Li, **H. Månefjord**, P. Travers, J. Salvador, L. Müller, D. Dreyer, J. Alison, T. T. Høye, G. Hu, E. Warrant, M. Brydegaard, (Accepted, 2024) "*Lidar as a Potential Tool for Monitoring Migratory Insects: A Field Case Study in Sweden*" Iscience

1 Introduction

The strive to understand and measure our world has always been part of human curiosity. Consider the questions in agriculture: What factors influence our crop yields and food production? Or in ecology: What mechanisms shape and influence the natural environments we inhabit? In the pursuit of answers, science has evolved and built upon itself for millennia. Complementing methods like visual inspection, dissection, and taxonomy [1, 2], optical instrumentation such as microscopes, spectrometers, and lidars are used in the field of biophotonics to expand our knowledge.

In biophotonics, light is used to diagnose or treat the living. Biophotonics is multidisciplinary, at the intersection of physics, biology, engineering, chemistry, and medicine. Biophotonic techniques are, for example, used to analyze the scattering of blood, study plant health, and monitor insect biodiversity. In this thesis, these inquiries will be examined using novel biophotonic instrumentation.

The possibilities to conduct biophotonic measurements vary over the world depending on available funds and access to advanced equipment. Many regions with low research funding have local issues with insect-borne diseases and agriculture that are threatened by climate change. Yet, these regions often lack the possibility to carry out essential research for the benefit of their communities with cutting-edge instrumentation.

Hence, there is a great opportunity to expand their research possibilities by developing low-cost, open-source, modular, biophotonic instruments that are easy to replicate and use in field studies. Therefore, the biophotonic instrumentation designed within the frames of this thesis has an explicit goal to be *accessible*.

1.1 Research overview and structure

This thesis aims to contribute to the field of biophotonics by developing and showcasing applications of novel low-cost biophotonic instrumentation. The specific objectives for the thesis are threefold:

The first objective is the design of four accessible instruments, detailed in Papers I-IV. The instruments "BIOSPACE" (biophotonics, imaging, optical, spectral, polarimetric, angular, and compact equipment) and "SWIR BIOSPACE" (short wave infrared biophotonics, imaging, optical, spectral, polarimetric, angular, and compact equipment), described in Paper I and IV are modular multi-dimensional cameras built with LEGO® and 3D-printed components. They excel with their versatility of being able to conduct multiple types of measurements with the same instrument. Papers II and III describe 3D-printed hyperspectral lidars named fluorescence hyperspectral lidar (FHSL) and elastic hyperspectral lidar (EHSL). They stand out by having the greatest number of spectral bands of any lidar, to our knowledge.

The second objective, covered by Papers V-IX, is the reporting of applications and data processing techniques for the instruments. Insect-related results include finding the activity pattern of two species of stingless bees with a temporal resolution not previously achieved. Also, the wing thickness of a flying insect was measured remotely for the first time with a lidar. In vegetation applications, leaves from locally important crops were classified and their health status was investigated remotely with a hyperspectral lidar. A finding was that the upper side of the leaves showed more contrast for species detection while the lower side of the leaves differed more depending on plant stress.

The final objective involves discussing the accessibility and educational perspectives of the instruments which was done in Papers X and XI. Table 1.1 states each paper's primary research focus area and Table 1.2 provides a detailed matrix categorizing the papers based on both their research focus areas and their methodological approaches.

Table 1.1. Each paper of the thesis listed within their primary research focus area.

Instrumentation	Insects	Vegetation	Perspectives
Paper I. A biophotonic platform for quantitative analysis in the spatial, spectral, polarimetric, and goniometric domains	**Paper V.** High-resolution activity patterns of African stingless bee species monitored with hyperspectral lidar	**Paper VII.** Low-Cost and Lightweight Hyperspectral Lidar for Mapping Vegetation Fluorescence	**Paper X.** BIOSPACE–A low-cost platform for problem-based learning in biophotonics
Paper II. 3D-printed fluorescence hyperspectral lidar for monitoring tagged insects	**Paper VI.** Insect Stratification & Diversity Across Taï Virgin Forest Canopy, Côte d'Ivoire – With Entomological Lidar	**Paper VIII.** Remote Vegetation Diagnostics in Ghana with a Hyperspectral Fluorescence Lidar	**Paper XI.** Towards global insect biomonitoring with frugal methods
Paper III. Remote Nanoscopy with Infrared Elastic Hyperspectral Lidar	**Related work XII.** Lidar as a Potential New Tool for Monitoring Migratory Insects	**Paper IX.** Mapping of Algae on Walls with a 3D Printed Hyperspectral Fluorescence Lidar	
Paper IV. SWIR Mosquito Characterization			

Table 1.2. A matrix categorizing the papers based on what research focus areas and methodological approaches they feature.

	Instrument design	Entomology	Vegetation	Pedagogical perspectives
Lidar	Paper II, III	Paper II, III, V, VI, XI, RW. XII	Paper VII-IX	Paper XI
Imaging	Paper I, IV	Paper I, IV, VI, XI	Paper X	Paper X, XI
Spectroscopy	Paper I-IV	Paper I-VI, XI	Paper VII-X	Paper X, XI
Polarization	Paper I	Paper I, VI, XI		Paper X, XI
Goniometry	Paper I, IV	Paper I, IV, XI		Paper X, XI

2 Background

2.1 Insects

Insects are the most diverse and abundant group of animals, estimated to number 10^{19} across approximately one million documented species. Entomology (the study of insects) investigates insects' roles as pollinators, sources of food, and key contributors to terrestrial biodiversity [3, 4].

As the primary pollinators in most ecosystems [5], bees, including the western honeybee (*Apis mellifera*) and various genera of stingless bees (*e.g.*, *Meliponula*) in tropical regions, are vital for agriculture [6, 7]. The decline of bees, and insects in general, poses catastrophic consequences for both biodiversity and agricultural production [8-12]. Insects also play a role as pests, inflicting significant damage in forestry [13] and agriculture [14]. For example, the spruce bark beetle (*Ips typographus*) has killed millions of spruce trees in European forests [15, 16]. Another significant aspect of insects is their role as disease vectors. Mosquitoes are the deadliest animals on earth, responsible for over half a million deaths annually by spreading diseases such as malaria, dengue fever, yellow fever, Zika, and encephalitis [17].

Established methods of field measurements often involve capturing insects using sweep nets or traps [18]. These traps may employ attractants such as pheromones [19], carbon dioxide (CO_2) [20], or light [21], which, while increasing catch numbers, also introduce biases. Baitless traps, like malaise traps, do not eliminate bias either, as they primarily capture flying insects less likely to escape [22]. These conventional methods generally require manual effort from skilled professionals to identify catches, either through visual inspection or genetic sequencing [23]. Trapping and sweep netting have been used as ground truthing in the work presented in Paper VI, see Figure 2.1.

Biophotonics investigations of insects can provide entomological insights, such as aiding in species determination for visually identical species [24], assessing insects' wing thicknesses [25], or whether they are gravid [26]. Insects have an exoskeleton consisting of the polymer chitin which is hardened in a process called sclerotization and combined with the dark pigment melanin in a process called melanization [27]. The main chromophores in insects that absorb light of different wavelengths are melanin and water. However, the diverse colors of many insects are not the results of pigments but instead structural colors from nanostructures of chitin and melanin in their exoskeleton [28].

Figure 2.1. (Left) Lauro and Meng are emptying two malaise traps in the Taï rainforest, Côte d'Ivoire. One trap was at ground level and one at 20 m height in the canopy. (Right) Some of the insect catches from the traps are pinned for photographing and wing characterization. The inventorying served as ground truth data for insect lidar data at different heights in Paper VI.

2.2 Vegetation

Plant biodiversity is foundational to life on Earth [29]. Vegetation plays a critical role in regulating the Earth's climate and contributes significantly to carbon cycling and hydrological processes. It defines local habitats by providing structure, shelter, and food, while also contributing to overall biodiversity. The widespread decline in plant biodiversity is a concerning phenomenon observed across various habitats and geographic regions [30, 31].

The study of vegetation has advanced over time, incorporating a range of techniques to understand plant physiology and structure. Sampling methods include field surveys, transect sampling, and quadrant analysis [32]. Subsequent analyses may involve visual inspection, genetic analysis, or biophotonic approaches such as spectroscopy and fluorescence imaging, providing insights into the health and composition of vegetation. Leaves are structured in multiple layers (Figure 2.2) that contain chemical compounds that interact with light through various processes, further explored in Section 3.3. The advancements in biophotonic methods [33] have expanded our capabilities, allowing remote sensing to gather vegetation data at large scales.

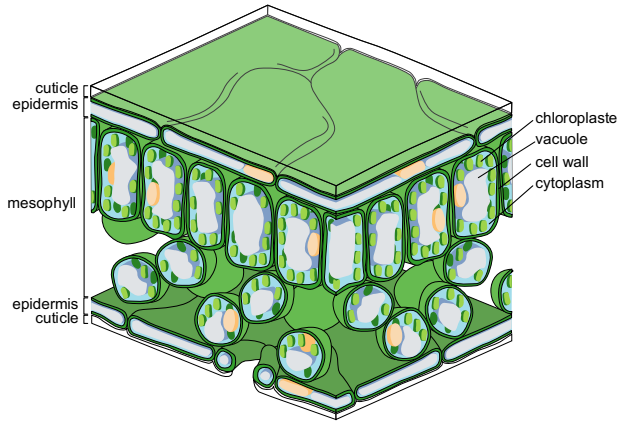

Figure 2.2. Schematic of the inside of a leaf. The cuticle is a non-cellular protective layer that contains waxes and oils that cover the entire leaf surface. The epidermis is the outermost cell layer of the leaf, which provides mechanical strength to the leaf and regulates the exchange of water and carbon dioxide to the surroundings. The mesophyll is the bulk tissue of the leaves that contains many of the chemical compounds of interest for biophotonic investigations. Water accounts for 50-90% of the mass of the leaves and is mainly located in the vacuoles and cytoplasm of the mesophyll. The photoactive molecules responsible for photosynthesis, chlorophyll, and carotenoids are located in the chloroplasts of the mesophyll [34]. Image attribution [i].

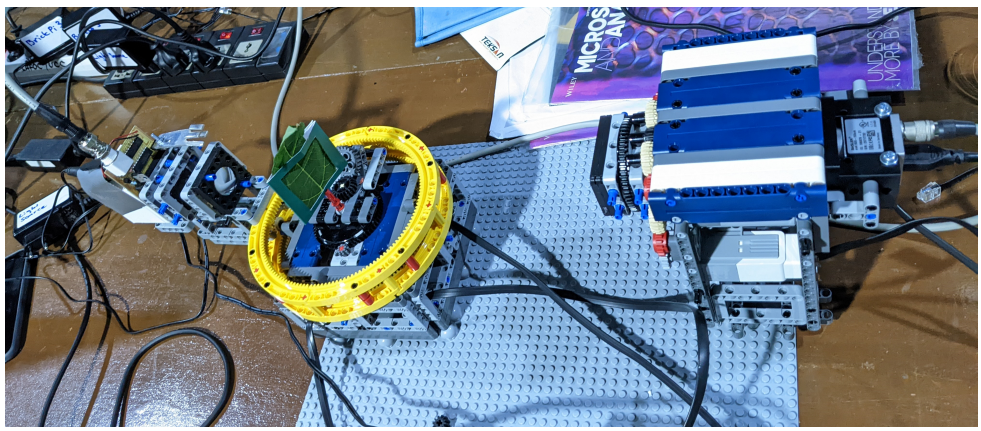

Figure 2.3. The optical properties of a leaf were measured with BIOSPACE during a workshop at the University of Cape Coast, Ghana. During this workshop two replicates of BIOSPACE were built and one copy of the FHSL.

Figure 2.4. A remote fluorescence measurement of a tree canopy at the campus of the University of Cape Coast, Ghana. The canopy structure was scanned at the same time as fluorescence measurements from the leaves were acquired as part of Paper VIII.

2.3 Remote sensing

With our eyes and ears, we constantly gather information about the world without physical contact. This means that we are constantly remotely sensing. For scientific measurements, specific instruments are used to quantify information on large scales using satellites, airplanes, drones, or terrestrial instruments [35].

Remote sensing can be categorized into two methods: passive and active. Passive remote sensing probes signals generated by an external source, typically the Sun. The sunlight interacts with the objects under observation, and the returned signal is measured. These signals could come from an insect's beating wings [36] or from a forest canopy [37]. In passive remote sensing, the observer has no control over the source. In contrast, in active remote sensing, the source is part of the instrument. Energy is sent as some form of radiation, in nature it can be an ultrasound pulse from a bat, or a red searchlight beam sent out by the deep-sea fish called stoplight loosejaw. In both these examples the sent signal is invisible to the prey. The radiation from active remote sensing instrumentation can range from microwave signals from radars to light flashes from cameras and beyond. Regardless of its form, the radiation interacts with the target and returns to the observer, providing information of the target. The category of remote sensing that forms the focus of this thesis is *active* and *photonic* (*i.e.*, using light), in part for laboratory measurements, and in part for remote sensing in the field, specifically with light detection and ranging (lidar).

The initial application of lidar in the 1930s involved atmospheric measurements using searchlights [38]. However, the invention of the laser in 1960 [39] enabled laser-based active remote sensing [40].

In entomology, lidar has been used to detect insects from distances of several kilometers away [41] and to monitor insect abundance, biomass, and distribution [42-44]. Specific parameters of insect behavior have been reported, such as flight direction and velocity [25, 45-47]. Lidars have also been used to identify species and sex [48, 49] of insects and to assess whether they are gravid [26]. Other active entomological remote sensing methods include radio detection and ranging (radar). Radars have been successfully employed in entomological research [50-52], offering advantages over lidars such as robustness, non-supervised operation, and extensive area coverage. Their limitations include extended near limits, problems with ground clutter, and limited resolution [53]. Additionally, the spectroscopic possibilities of lidars, which will be explored in this thesis, are beyond the scope of radar technology.

In vegetation analysis, passive remote sensing often involves multi- or hyperspectral imaging, which can reveal signs of vegetation stress [54, 55] and diseases [34, 56]. Solar-induced fluorescence (SIF) is an important proxy for photosynthetic activity and can be measured by probing wavelengths where sunlight intensity is low due to atmospheric absorption, typically at the oxygen absorption bands or Fraunhofer Lines [57]. These passive methods can rely on satellite imagery and thus provide global coverage [58]. Active methods include radar [59, 60] and vegetation lidars. Multispectral vegetation lidars have proven effective in classifying tree species [61, 62] with the benefit of also providing depth information that contributes significantly to forest characterization [63]. Vegetation lidars can thus estimate biomass distribution and map canopy structure [64-71]. Such measurements of canopy structure have been reported to correlate with the species richness of birds and insects [72, 73].

In this thesis, I expand on the capabilities of lidars in both entomology and vegetation. My work includes analyzing lidar-detected insect wingbeat frequencies and wing thickness, tracking insects using fluorescence tagging, and examining differences in fluorescence signatures, depending on species and health status. These applications showcase the versatility of lidar in studying insect behavior and vegetation health.

Figure 2.5. A long exposure photo of vegetation fluorescence scanning experiment along a forest edge at Stensoffa field station, Sweden. From the scan a point cloud could be reproduced were each point has a full fluorescence spectrum, as part of Paper VII. Image attribution [ii].

Figure 2.6. Meng, Adolphe, Doria, Mikkel, and Benoit by the lidar, conducting remote sensing of insects in Taï rainforest, Côte d'Ivoire, as part of Paper VI. The motorized tripod was programmed to sweep to different angles, so different heights of the canopy were probed.

2.4 Open-source instrumentation and frugal science

"*Copying all or parts of a program is as natural to a programmer as breathing, and as productive. It ought to be as free*".

– Richard Stallman, 2002

The sharing of information has existed throughout history; indeed, the emergence of the first libraries 5,000 years ago marks the transition from prehistory to history [74]. Such institutions and corresponding practices laid the groundwork for collaborative knowledge enhancement, a principle at the heart of open source. The term *open source* itself emerged during the late 1990s, addressing the need for a less ambiguous word than "free software" previously used in the early movements to guarantee end users' freedoms to access, use, modify, and distribute programming code. Open-source software is typically accompanied by a so-called *copyleft* license which outlines the obligations of the end users. These obligations vary among licenses but generally include the stipulation that all derivative works must be distributed under the same copyleft license [75, 76].

Building on the principles of open-source software, the open-source hardware movement applies open-source licenses to electrical schematics, 3D-printing designs, component lists, and blueprints. This practice is prevalent in devices such as 3D printers, including RepRap and Ultimaker; as well as microcontrollers and single-board computers like Arduino, SparkFun Electronics, and Raspberry Pi. The scientific community actively contributes to this trend [77, 78]. Similarly, the concept of *open access* in academia embodies the principle of making research outputs freely available to everyone [79]. However, the free availability of open-access publications in academia often comes at the expense of hefty publishing fees, moving the costs from the consumer to the producer.

Improving the accessibility of science also depends on reducing the cost of scientific instrumentation. Frugal science, as discussed in Paper XI is addressing affordability, accessibility, and sustainability. Reducing costs and innovating by subtraction [80] is particularly important in regions with lower income levels where science is more limited by funding and thus less represented. The underrepresentation of science in these areas constitutes opportunities for advancements with low costs. Open-source software and hardware are important tools in democratizing access to research instrumentation.

This thesis project aims to benefit, and include contributions from the low- and middle-income regions [81]. Workshops, sharing of instrumentation, and collaborative production of papers have been conducted with collaborators in universities in Ghana, Côte d'Ivoire, and Ecuador. Furthermore, all code and designs from this project are published under open-source licenses, available on GitHub [82-86], and the papers are available through open access.

Figure 2.7. Justice, Andrew, Rabbi, Hampus (the author), and Benjamin replicating BIOSPACE in a workshop at the University of Cape Coast in Ghana. Lego sets and a 3D printer were brought to the university to fully replicate the instrumentation on site. Image attribution [x].

3 Light

"*Let there be light.*"

– God, 4 004 BC

Light from the Sun is one of the most fundamental drivers for life on our planet. Despite its essential role, the nature of light and its interactions with matter are complex and an active research field. This chapter delves into some of these intricacies, describing light through different representations and detailing its properties and interactions. Understanding these properties and how light interacts is crucial for designing biophotonic instrumentation that at its core manipulates and analyzes light for scientific advancements.

3.1 Light representations

3.1.1 Light as rays

As children, we draw the sun with rays extending in all directions. The intuition of light behaving as rays could be described as simple by many physicists, but as we will see, it proves to be quite useful.

The earliest mathematical treatment of light traces back to Euclid in the 300s BC, laying the foundation for what would become the field of geometrical optics. Over the centuries, this field has been refined and expanded [87]. In geometrical optics, light is described as rays that emanate from a light source and travel to a detector. The speed of light (c) through any medium is characterized by the refractive index, n, given by $c = \frac{c_0}{n}$, where c_0 is the speed of light in vacuum. According to Fermat's principle, light travels along the path where time is at an extreme (usually minimized). In homogenous media, this path is straight, it curves in graded-index media and bends at an angle when moving between media with different refractive indices. Light traveling in scattering media complicates this concept with probabilistic scatter events, resulting in paths resembling random walks in the particle representation of light. These paths can be modeled with light transport equations or Monte Carlo methods that can be solved numerically for different geometries.

Based on geometrical optics, instruments such as telescopes and microscopes have been constructed [88]. With modern computers, ray-tracing (see Section 5.1) software now enables the simulation of light rays to optimize complex optical systems, as utilized in the design of FHSL and EHSL in Papers II and III. However, while powerful, geometrical optics do not account for certain properties of light, such as interference, diffraction, and polarization, which are better explained by the wave and particle models.

3.1.2 Light as waves

Light is often more accurately described as a wave, a concept theorized by Huygens [89] and empirically demonstrated by Young's double-slit experiment in the 19th century [90]. In wave optics, light is characterized by a complex wave function $U(r,t)$ where r denotes the position and t represents time. This wave function is one solution to the wave equation,

$$\nabla^2 U - \frac{1}{c^2}\frac{\partial^2 U}{\partial t^2} = 0 \qquad 3.1$$

where ∇^2 is the Laplacian operator. Solutions to the wave equation vary depending on the boundary conditions. For example, a monochromatic wave can be described by the wavefunction $U(r,t) = U(r)\, e^{-i2\pi t/\lambda}$, where λ is the wavelength of the light and $U(r)$ is the complex amplitude, representing the wave's amplitude and phase.

Ray optics is most applicable when the light's wavelength is significantly smaller than the objects it encounters. Conversely, the wave characteristics of light become more evident with longer wavelengths [91]. The wave model accounts for phenomena such as polarization as explored in Papers I, VI, X, and XI, and diffraction, as utilized with gratings in the design of the FHSL and EHSL. However, the wave model is limited in explaining light absorption, which is dependent on the wavelength rather than the amplitude of the light wave.

3.1.3 Light as particles

Light can be described as discrete packets of energy known as photons, a particle without mass but with momentum. This particle description of light arose in the early 20th century and is crucial for explaining phenomena such as Einstein's photoelectric effect [92], as well as understanding the absorption (μ_a) and scattering (μ_s) coefficients, which are vital in modeling light transport in turbid media, as explored in Paper I.

3.2 Light properties

Light possesses a set of distinctive properties: localization, propagation direction, intensity, wavelength, phase, and polarization state. Optical measurements involve assessing how these properties of light are altered during interactions with matter, thereby allowing us to draw conclusions about the material under investigation.

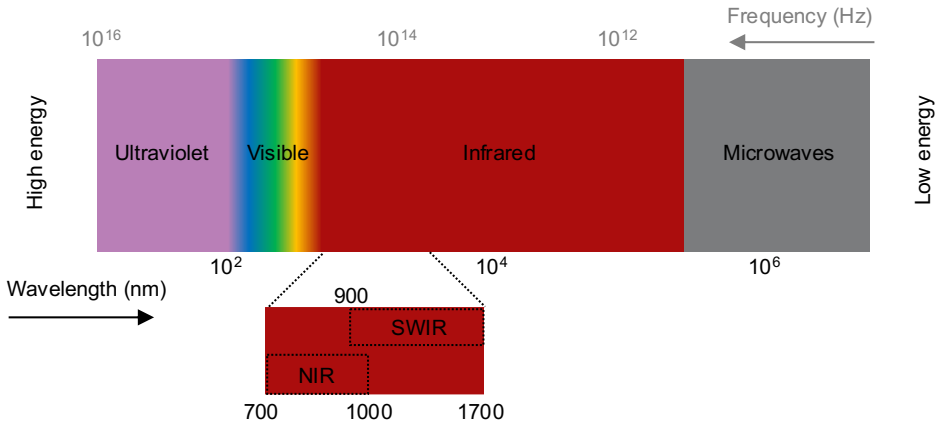

Figure 3.1. Wavelength and frequency ranges for ultraviolet (100-400 nm), visible (400-750), near infrared (700-1000 nm), shortwave infrared (900-1700 nm) light.

The intensity of light (I) represents the power transferred per unit area measured in W/m^2. This is proportional to the ray- or photon density in the ray and particle models, and to the square of the complex amplitude $I \propto |U|^2$, in the wave model. Variations in intensity are a measure that can probe, *e.g.*, changes in optical cross sections, which is used in the work presented in Papers III and VI to deduce insect wing beats from lidar time series signals.

The wavelength, λ (nm), of light, is inversely proportional to both the frequency, ν (Hz), from the wave model and the photon energy E_{photon} (J) of the particle representation,

$$E_{photon} = h\nu = hc_0/\lambda \tag{3.2}$$

where h is Planck's constant. Spectroscopy, *i.e.*, the study of light wavelengths, provides vital information about material interaction processes, including molecular constituents, and features in all papers of this thesis. Wavelength and frequency ranges for ultraviolet, visible, near infrared (NIR), and shortwave infrared (SWIR) light are shown in Figure 3.1.

The phase of light corresponds to the relative stage of the oscillating electromagnetic wave. Constructive and destructive interference result from light waves that are in or out of phase, respectively. The phase of light can thus be measured indirectly with

interferometric methods. In this thesis work, such interference measurements were made to estimate the thickness of insect wings, as reported in Papers I, III, and IV.

The polarization of light corresponds to the path of the electric field vector over time. This vector lies in a plane tangential to the propagating light, tracing an ellipse known as the polarization ellipse. The polarization of light is fully described by the size, orientation, shape, and handedness of this ellipse and can be mathematically expressed using coordinates on the Poincaré sphere, Stokes parameters, or complex Jones matrices [91]. Linear and circular polarization represent two common extremes of the polarization ellipse, as illustrated in Figure 3.2. Considering linearly polarized light impinging on a surface, its polarization angles are affected differently; s-polarized describes light with its electric field perpendicular to the plane of incidence, while p-polarized is parallel to the plane of incidence.

A full characterization of the polarization state of light is rarely available. In biophotonics, a common metric is, instead, the degree of linear polarization ($DoLP$), which measures the proportion of light that maintains its original linearly polarized state, I_{copol}. $DoLP$ has several definitions, but the one used in this thesis is,

$$DoLP = \frac{I_{copol}}{I_{copol} + I_{depol}} \tag{3.3}$$

where I_{depol} is the intensity of light with orthogonal polarization to I_{copol}. Hence, a $DoLP = 1$ indicates completely copolarized light, while $DoLP = 0.5$ describes unpolarized light. In this thesis work, polarization is examined in terms of $DoLP$ in Papers I, VI, and X-XI.

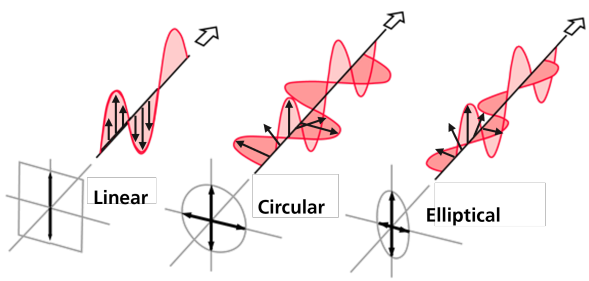

Figure 3.2. Linear circular and elliptical polarization of light. The arrows show the oscillations of the electric field as the light propagates. Image attribution [iii].

3.3 Light interactions with insects and vegetation

The interplay of light and organic tissue involves complex phenomena. When encountering insects or vegetation, light undergoes reflection, refraction at boundaries, and scattering, absorption, and subsequent fluorescence within the media. Figure 3.3, illustrates these interactions which are strategically utilized by organisms. Insects create structural colors in their exoskeletons [93] and wings [94] for mate attraction [95] and thermoregulation [96]. Plants absorb and fluoresce light as part of photosynthesis, and use colorful patterns on petals to guide pollinators [33].

Beyond visual roles, understanding light interactions enables the assessment of insect and plant health. Wing thickness can be deduced from interference patterns [25], while plant stress [54, 97], disease [56], and growth [98-100] can be assessed by reflection and fluorescence signatures.

In the following sections, these light interaction processes will be explored in more detail. Their impact on the biological characteristics of insects and plants, as well as their significance for scientific observation and analysis, will be highlighted.

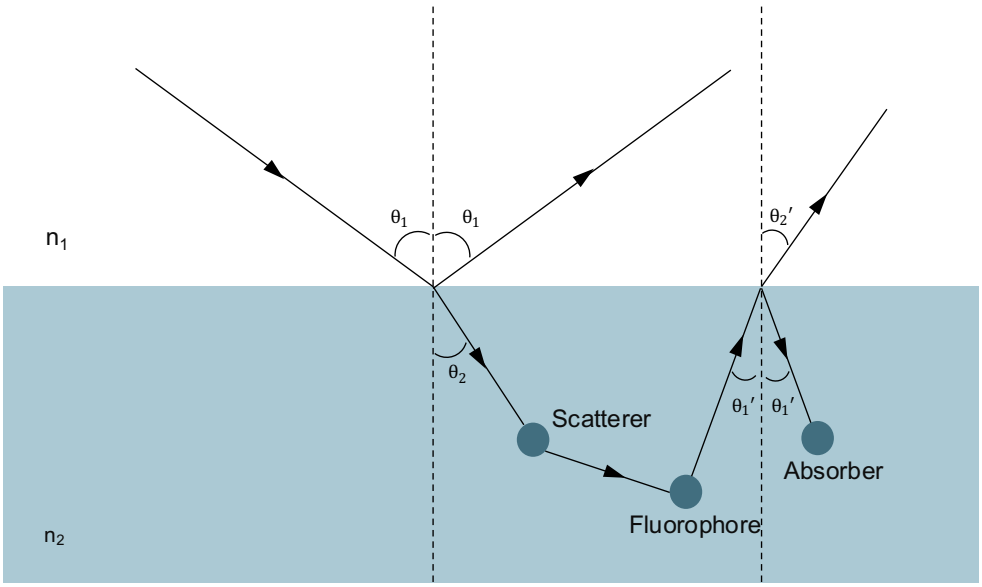

Figure 3.3. Illustration of how light interacts with turbid media. Incoming light is reflected, refracted, scattered, absorbed, and reemitted as fluorescence. Part of the fluorescence escapes the media with a final refraction and the other part is internally reflected and absorbed. The properties of the light change through these interactions; the propagation direction, as illustrated, but also the polarization state and wavelength of the light is changed through fluorescence and can be through scattering depending on the process.

3.3.1 Reflection and refraction

When light transitions from one medium to another with differing refractive indices (n_1 and n_2) it typically undergoes both reflection and transmission (Figure 3.3). Incident light striking the boundary at an angle θ_1 reflects at an equal angle relative to the surface normal. Transmitted light refracts at an angle θ_2 as described by Snell's law [42],

$$n_1 \sin(\theta_1) = n_2 \sin(\theta_2) \tag{3.4}$$

Refraction is responsible for the focusing effect that lenses have in optical systems. Similarly, leaves in low light conditions utilize the refraction of their epidermal cells to focus more light into the leaf's interior [101].

A material's refractive index depends on the light's wavelength and relates to its absorption frequencies via the Kramers-Kronig relations. Wavelengths that are longer than the nearest absorption peak exhibit a decreasing refractive index with increasing wavelength. This is the case for many materials throughout the whole visible region due to strong UV absorptions, including water, chitin, and melanin which constitute the bulk of insects [102] (Figure 3.4). However, the chlorophyll of leaves has strong blue and red absorption peaks, and therefore leaves show increasing refractive index for those spectral regions [33] (Figure 3.4).

The differences in refractive indexes also influence the amount of reflected and transmitted light, with larger differences between n_1 and n_2 yielding higher reflection (R). For normal incidence, the reflection and transmission (T) are:

$$R = \left|\frac{n_1 - n_2}{n_1 - n_2}\right|^2 \qquad T = 1 - R \tag{3.5}$$

For light striking at an angle, both the incidence angle and the polarization of the light affect the relative reflected intensity, as described by the Fresnel equations,

$$R_s = \left(\frac{n_1 \cos\theta_1 - n_2 \cos\theta_2}{n_1 \cos\theta_1 + n_2 \cos\theta_2}\right)^2 \qquad T_s = 1 - R_s \tag{3.6}$$

$$R_p = \left(\frac{n_2 \cos\theta_2 - n_1 \cos\theta_1}{n_1 \cos\theta_1 + n_2 \cos\theta_2}\right)^2 \qquad T_p = 1 - R_p \tag{3.7}$$

where R_s and T_s represent the relative intensities of reflected and transmitted s-polarized light, and R_p and T_p correspond to the relative intensities of p-polarized light [91].

Reflection from leaves and insects is further complicated due to surface features. Leaves have hair which in some species, such as desert plants, can make leaves appear white instead of green, resulting in a favorable energy balance for the plants [33]. Similarly, insects have microstructures that regulate their temperature [96] and

nanostructures that create iridescent effects of different wavelengths being reflected depending on incidence angles [28].

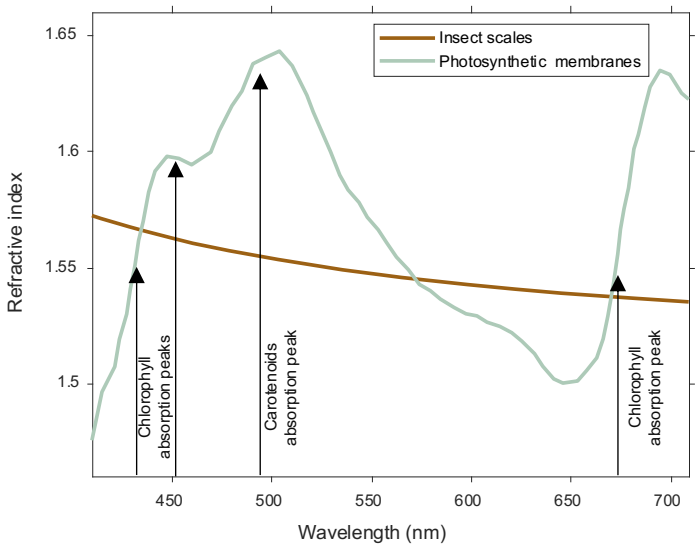

Figure 3.4. The refractive index of the scales of the common bluebottle butterfly (*Graphium sarpedon*) adapted from [103] is decreasing for increasing wavelength due to UV absorptions. The photosynthetic membranes show increasing refractive index near the absorption peaks of the contained chlorophyll and carotenoids, adapted from [33].

3.3.2 Absorption

Absorption is the process of a material taking up a photon's energy, causing its electrons to transition to a higher energy level (Figure 3.5a). It is wavelength-specific: only light with wavelengths matching the material's energy transitions will be absorbed, while light of other wavelengths passes through. The intensity (I) of light remaining after traveling a distance (l) through an absorbing medium follows the Beer-Lambert law:

$$I = I_0 e^{-l\mu_a} \qquad \textbf{3.8}$$

where I_0 is the initial intensity and μ_a (m^{-1}) is the absorption coefficient [91].

Different compounds play critical roles in light absorption within biological systems. In leaves, chlorophyll, carotenoids, and water are the primary absorbers. Chlorophyll and carotenoids absorb blue and red light for photosynthesis, while water is transparent in the visible range but strongly absorbs NIR and SWIR wavelengths (Figure 3.6a) [33]. In insects, melanin and water are the dominant absorbers. Melanin absorbs broadly throughout the visible spectrum, with decreasing absorption at longer wavelengths.

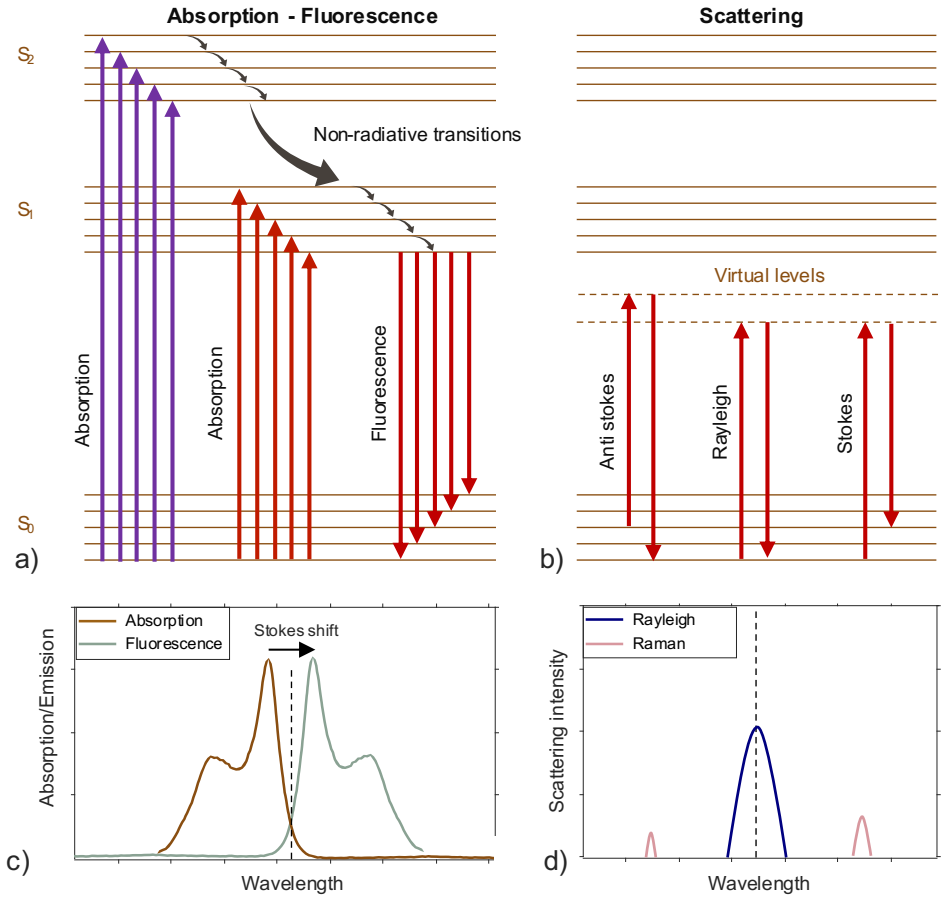

Figure 3.5. a) Absorption of photons results in transitions from the ground state S_0 to the exited electronic states S_1 and S_2. When the excited state has many vibrational levels absorption can be achieved over a broad spectral range. After non-radiative transitions in photons can be re-emitted as fluorescence with less energy, b) Scattering of photons excites electrons to short-lived virtual levels after-which a photon is re-emitted. For Rayleigh scattering the energy is conserved while for Stokes and anti-Stokes Raman scattering the emiited photon has different energy since it either starts or ends in a higer vibrational level of S_0. The wavelength of the scattered photon is shifted accordingly. c) The shape of the absorption spectrum corresponds to the probability of excitement to the different vibrational levels of S_1 and S_2, and the fluorescence spectrum correspond to the different levels the ground state. The fluorescence is thus a mirror image of the absorption with a so-called Stokes shift toward longer wavelengths. d) The elastic Rayleigh scattering has high intensity compared to the inelastic Raman scattering which wavelength has shifted according to the vibrational levels of the ground state.

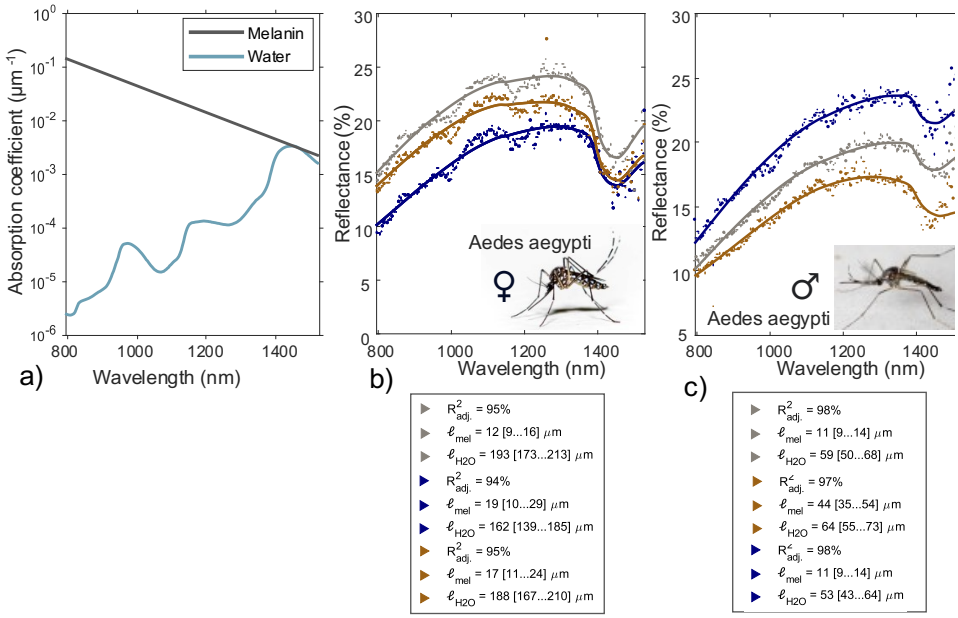

Figure 3.6. a) The absorption coefficients of water and melanin, the main absorbers for insects. b,c) Model from Paper IV fitted to the measured spectra of three female and three male *Aedes aegypti*. The estimated pathlengths (ℓ_{mel} and ℓ_{H2O}) are reported with error margins and goodness of fit (R^2_{adj}). The mosquitoes were bred at Sveriges Lantbruksuniversitet (SLU) in Alnarp and measured with a hyperspectral push-broom camera in a laboratory in Lund.

The absorption coefficients of melanin and water (Figure 3.6a) are valuable tools in spectroscopic models to estimate optical path lengths. The age of mosquitoes has been shown to affect the NIR absorption spectrum [104] and Paper IV expands on this application by comparing mosquitoes of different species, sexes, and ages by estimating their optical path lengths. Figure 3.6b-c showcases the measured spectra of *Aedes aegypti*, a mosquito known to transmit yellow fever, Zika, and dengue viruses, alongside the fitted melanin and water path lengths derived from the measurements reported in Paper IV. Here, the model shows shorter water path lengths in male *Aedes aegypti* compared to females.

3.3.3 Fluorescence

A fluorescent material (fluorophore) can re-emit absorbed photons at longer wavelengths after losing energy through non-radiative transitions. This light is called fluorescence and typically has a broad spectrum, characteristic of the material's energy levels. The spectral shape is a mirror image of the absorption spectrum, red-shifted with a so-called Stokes shift (Figure 3.5a,c). Fluorescence created inside a medium is once again subject to absorption before reaching a detector. If the wavelength of the fluorescence overlaps with any absorber in the medium, this process is called reabsorption and is illustrated in Figure 3.3. If the absorber is a fluorophore, light can

be emitted again, altering the fluorescence spectrum and complicating intrinsic fluorescence measurements due to emission quenching [105].

The FHSL developed in this thesis project (Paper II) has the capability of detecting fluorescence remotely. This was used to monitor the activity patterns of honey bees in Sweden and Stingless bees in Ghana tagged with fluorescent powder, see Paper II and Paper V.

Examples of fluorophores are found in everyday life, such as highlighting pens and laundry detergents that convert UV light to enhance perceived whiteness. Fluorophores are also widely found in nature. The 2008 Nobel Prize in Chemistry was awarded to scientists for their work isolating a green fluorescent protein (GFP) from a jellyfish, which has since been widely used as a marker in cell biology [106]. Fluorescence also serves various functions across animal species. For example, the deep-sea siphonophore *Erenna sp.* uses fluorescent lures to attract prey, while certain insects utilize fluorescent markings for sexual selection [107].

My hosts during a research trip to Université de Paris Cité and Université Sorbonne, France, discovered a bright green fluorescence of Asian paper wasp nests [108]. Together we investigated and confirmed that characterization could be accomplished remotely by the FHSL. The paper wasp nests and other natural fluorescent samples were remotely measured. While our findings remain unpublished a selection of the measurements is presented in Figure 3.7 and Figure 3.8.

Figure 3.7. a) The hyperspectral lidar in Seine-Port, France measuring autofluorrescence at 25 m distance in daylight. b) *Polistes brunetis* nest fluorescing in bright green. d) Photo of the measured cocoon illuminated with violet laser light. e) The *Palomena prasina* eggs being measured with the lidar. f) The *Palomena prasina* eggs show the same hue of green in reflectance, while their fluorescence spectra are drastically different, see Figure 3.8.

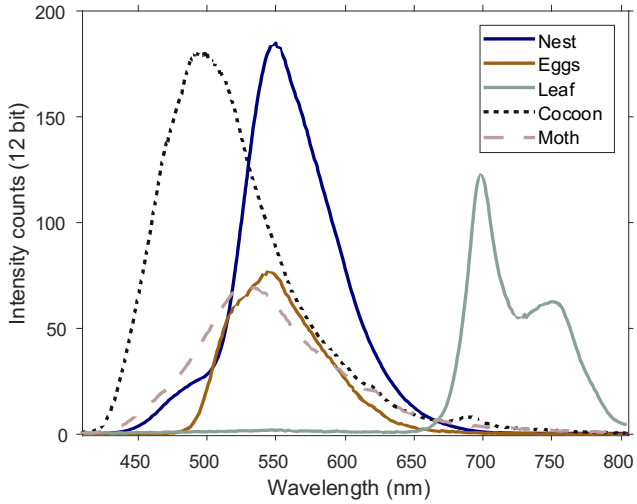

Figure 3.8. Fluorescence spectra of *Polistes brunetis* nest, *Palomena prasina* eggs, the lower side of a leaf, a cocoon and moth. The spectra are acquired remotely with the FHSL and correspond to the samples in Figure 3.7. The samples show spectacular contrast in fluorescence spectra even though they appear in similar hues of white, brown, and green in reflectance.

Plants possess various fluorophores, including chlorophyll, carotenoids, and waxes with broad absorption and emission bands resulting in emission quenching. Despite this challenge, vegetation fluorescence remains a powerful tool. It directly links to chlorophyll's role in photosynthesis and carbon assimilation, making it a valuable gauge for growth and an early indicator of stress [98, 109, 110]. Furthermore, the unique spectral signature of this fluorescence allows for species classification [111].

In the work presented in Paper VIII vegetation fluorescence of crops in Ghana was measured. Both the upper and lower sides of the leaves were measured, see Figure 3.9. Our results suggest the upper side exhibits greater spectral differences with health status, while the lower side provides better species differentiation.

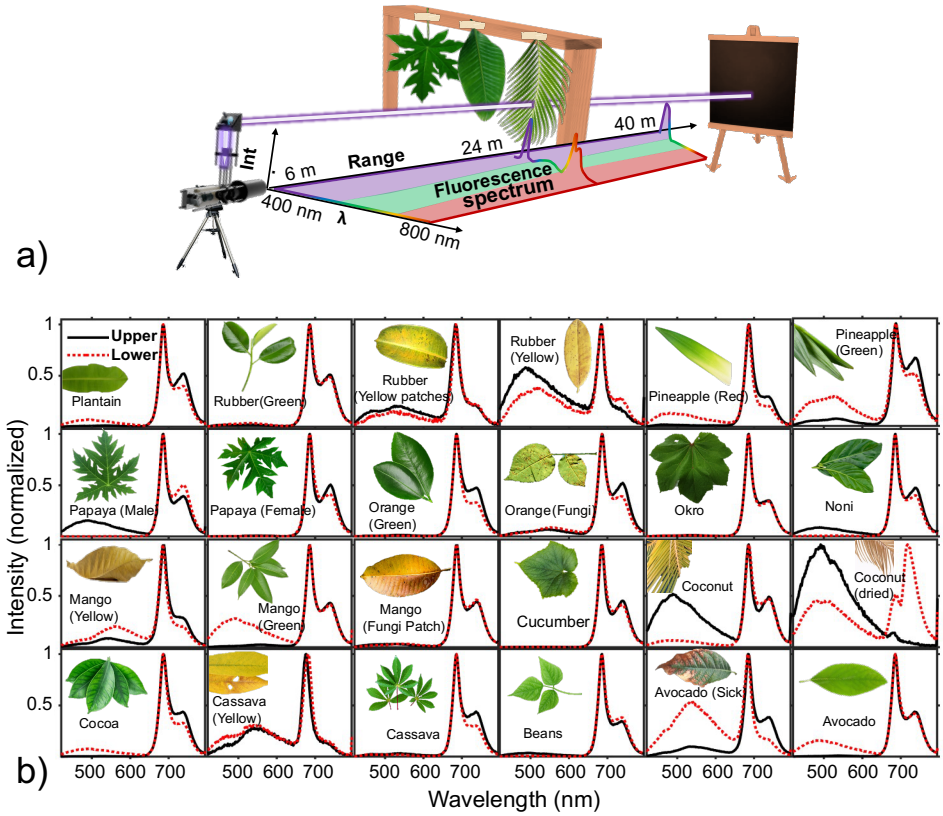

Figure 3.9. a) The upper and lower side of 24 leaves was scanned at 24 m distance with the FHSL. b) The fluorescence spectra of the leaves. The spectral shape varies between species, health status, and the probed side of the leaves.

3.3.4 Scattering

Light can interact with matter at off-resonance frequencies through a process called scattering, which changes the propagation direction. When the energy of the incident photon does not match the energy level difference required for absorption, electrons may still be exited to a short-lived *virtual state*, after which the photon is reemitted. If the reemitted photon has the same wavelength as the exciting one, the process is called Rayleigh scattering, and if it is altered, it is called Stokes or anti-Stokes Raman scattering. Find a schematic for the scattering process in Figure 3.5b and 3.5d. Rayleigh scattering has a much larger scattering cross section than Raman scattering, and both their scattering cross sections are proportional to λ^{-4} [112], indicating that light with shorter wavelengths has a much higher likelihood of scattering. This wavelength dependence explains why the sky is blue and sunsets are red.

For particles larger than the light's wavelength, Mie scattering dominates. Mie scattering arises from differences in refractive index and has a weaker wavelength dependence, roughly proportional to λ^{-2} [113]. Organic tissues, like those inside insects and leaves, are turbid media where light undergoes multiple scattering events. This randomizes its direction and polarization. The scattering coefficient (μ_s) defines the probability of scattering per unit distance within a material. It is possible to quantify μ_s with goniometers, as explained in Section 4.3.5.

Plants often benefit from high scattering, as it dramatically increases the optical path length of light within the leaf, enhancing absorption for photosynthesis [33]. Shade-adapted plants often demonstrate increased scattering for this reason [114].To appear white, intense multiple scattering is required, which for thin specimens such as small insects requires very high scattering coefficients. Examples of this are the extremely white beetles *Cyphochilus* and *Lepidiota stigma* which achieve their whiteness through optimized scattering structures and the highest reported scattering coefficients found in nature [115].

3.3.5 Interference, thin films, and iridescence

Interference occurs when two or more light waves with a relative phase shift combine through superposition. When light encounters a thin film, it reflects from both the front and back surfaces (Figure 3.11a). This reflected light can interfere constructively or destructively, depending on the film's thickness, the light's wavelength, and the angle of observation.

This phenomenon is responsible for the colorful reflections observed in soap bubbles and insect wings [93]. The spectrum from a thin film follows a fringe pattern described by [116]

$$R_{fringe} = \frac{4R^2 \sin^2\left(2\pi d\sqrt{n^2 - \sin^2\theta}\,/\lambda\right)}{(1-R^2)^2 + 4R^2 \sin^2\left(2\pi d\sqrt{n^2 - \sin^2\theta}\,/\lambda\right)} \qquad 3.9$$

where λ is the wavelength, d is the thickness of the wing, θ is the incidence angle R is the reflection coefficient according to Fresnel equations 3.6 and 3.7, and n is the refractive index of the film. In Paper III, this thin film model was used to remotely measure thicknesses of insect wings (Figure 3.10 and Figure 3.11). In Paper IV it was used to describe the thinnest insect wings reported, to our knowledge: *Anopheles stephensi* with 173 nm thickness.

Repeating structures with specific spatial frequencies cause strong interference, which is utilized in optical coatings and diffraction gratings, discussed in Section 5.1. In nature, insects use such structures to produce structural colors These structures often generate spectacular iridescent effects, where the perceived color changes with the viewing angle [28, 102].

Figure 3.10. The elastic hyperspectral lidar (EHSL) at Stensoffa field station, Sweden, measuring wing thicknesses of insects remotely. A flash in the laser beam indicates an illuminated insect. This work is included in Paper III. Image attribution [iv].

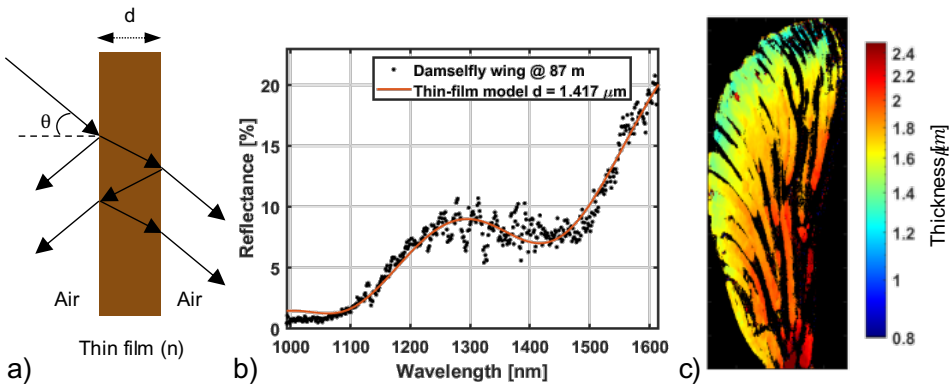

Figure 3.11. a) A schematic of light interference from thin films. b) Measurement and fitted fringe model of a damselfly wing measured at 87 m distance. c) Thickness of the same damselfly wing as in (b) scanned with a Hyperspectral push-broom camera. The thickness varies over the wing but corresponds to the remote measurement. This work is included in Paper III. Image attribution (b) and (c) [v].

4 Instrumentation

This section introduces light sources and detectors used in this thesis work. Then the principles of the developed instruments are explored. A compilation of the detecting and emitting spectral regions for the designed instruments is shown in Figure 4.1.

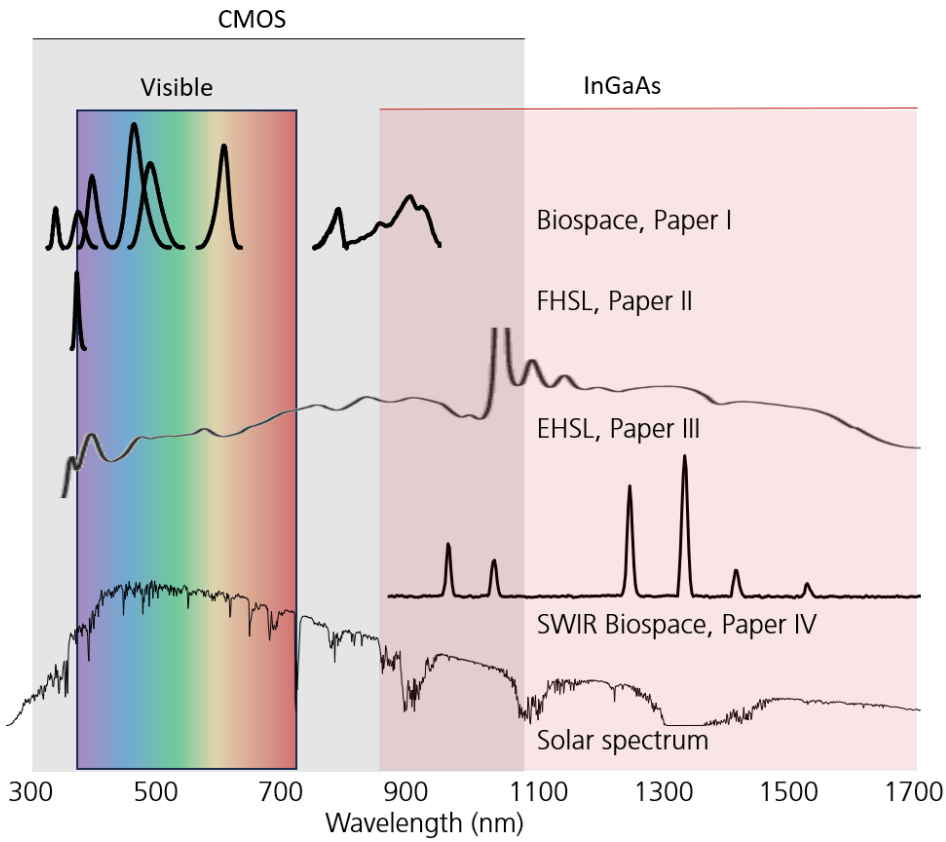

Figure 4.1. Emission spectra of the designed instruments during thesis work, including light emitting diodes, laser diodes, a supercontinuum source, and solar spectrum at sea level. The sensitivity regions of human eyes, CMOS image sensors, and InGaAs image sensors are indicated with colored rectangles.

4.1 Sources

4.1.1 Light-emitting diodes

Light-emitting diodes (LEDs) have become widespread as compact, affordable, and energy-efficient light sources. Initially available in the 1960s as Near Infrared (NIR) LEDs with low optical power, their development has since expanded to include visible [117], and ultraviolet (UV) wavelengths [118]. Over time, their optical power has increased, leading to widespread use in both everyday applications and scientific instrumentation [119].

LEDs consist of two doped semiconductors forming a p-n junction. A forward bias on the junction stimulates electron-hole pairs to recombine, emitting light, see Figure 4.2. The wavelength of the emitted light is determined by the bandgap of the doped materials.

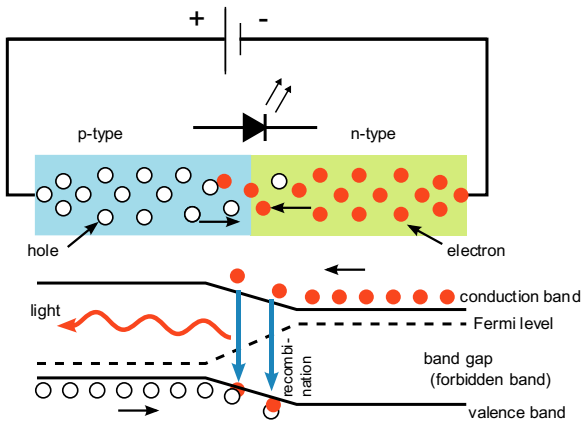

Figure 4.2. A schematic drawing of a p-n junction with a forward bias. Electrons in the conduction band recombine with holes from the valence bands producing photons. The wavelength of the emitted photon corresponds to the energy separation between the conduction band and the valence band.
Image attribution [vi].

The spectral width of the light emitted by an LED, denoted as $\Delta\lambda$ increases quadratically with the increasing central wavelength λ, $\Delta\lambda \propto \lambda^2$. The emitted light is incoherent and typically has a large divergence, which can be mitigated by collimating it with an appropriate lens. In BIOSPACE (Paper I), eight LEDs with wavelengths ranging from 365 nm to 940 nm were used to construct a multiplexed light source, further discussed in Section 4.3.3. Their respective spectra are shown in Figure 4.1.

4.1.2 Laser diodes

Laser diodes (LDs) were first demonstrated in the 1960s [91] and are today widespread due to their efficiency and their unique properties. They are similar in design to LEDs, based on doped semiconductors forming a p-n or p-i-n junction. While LDs function like LEDs at low currents, they include a gain region that, when supplied with current above a certain threshold, creates population inversion, amplifying the signal. The gain medium is encased in a cavity, which varies in form factor influences the divergence

angles of the emitted light. The function of this cavity is to reflect the spontaneously emitted light repeatedly, inducing stimulated emission in the gain medium. This process generates coherent light with uniform polarization and phase, with narrow spectral width and small beam divergence compared to non-laser sources [91]. The consistency of these properties in the emitted light is a defining feature of lasers and advantageous for biophotonics analysis. The small divergence of laser light allows long transects for remote sensing applications. In my research, a 405 nm laser was used in the lidar in the FHSL (Paper II), six laser diodes of wavelengths from 1002 to 1576 nm were used in SWIR BIOSPACE (Paper IV), and two 808 nm laser diodes were used in the work presented in Paper VI. For spectral shapes of these laser diodes, see Figure 4.1.

4.1.3 Supercontinuum light sources

Supercontinuum light sources were first demonstrated in the 1970s. They operate by propagating monochromatic light from a pump laser through a nonlinear medium, broadening the light into a continuous white spectrum. To achieve this extreme spectral broadening, high-power pulses are essential, often produced by mode-locked lasers emitting femtosecond or picosecond pulses. The concept of supercontinuum light sources was first demonstrated in the 1970s [120, 121]. In the research presented in this thesis, a supercontinuum light source pumped at 1064 nm and broadened to cover the range from 400 nm to 2400 nm, was utilized in the EHSL in Paper III, with its emission spectrum illustrated in Figure 4.1.

4.1.4 The Sun

The Sun illuminates the Earth with an average intensity of approximately 1 kW/m^2. Its spectrum can be approximated as that of a blackbody radiator, with a solar surface temperature of about 5778 K. This spectrum is modified by absorption from both the solar and Earth's atmospheres. The resulting spectrum (Figure 4.1), peaks in the visible region (~400 to 700 nm). This spectrum features both narrow Fraunhofer lines and broader absorption regions due to ozone (O_3) in the UV region, and vibrational transitions in water vapor (H_2O) and oxygen (O_2) in the NIR region.

Sunlight is often used for remote sensing applications. The atmospheric windows, where light is not significantly absorbed, are utilized in elastic remote sensing applications [47, 122]. Additionally, the Fraunhofer lines facilitate solar-induced fluorescence measurements [57]. In a master thesis [123], supervised as part of this thesis project, sunlight was used to identify the spectral characteristics of insect wings in the visible region. In other aspects of this thesis, sunlight constituted a background signal to be subtracted for accurate measurements.

4.2 Detectors

A photodiode is a semiconductor device that responds to light. Structurally similar to an LED, it typically features a p-n or more commonly a p-i-n junction. However, unlike LEDs, photodiodes are operated with reverse bias. Electron-hole pairs are generated through the photoelectric effect when incoming photons, matching the bandgap of the material, interact with the diode. Silicon-based photodiodes cover a wavelength range from UV to NIR (~350-1100 nm), while Indium Gallium Arsenide (InGaAs) photodiodes extend from NIR to SWIR (900-1700 nm) [124].

Arrays or matrices of photodiodes are known as complementary metal–oxide–semiconductor (CMOS) sensors. CMOS sensors feature a charge-integrating amplifier for each photodiode, as opposed to another form of image sensor called the charge-coupled device (CCD) sensor, which instead has a single amplifier. Over time, CMOS sensors have become increasingly popular, now found in nearly every smartphone. However, certain features of normal smartphone cameras make them less suitable for scientific experiments.

One such feature in standard image sensors is a rolling shutter mechanism, where each pixel in a frame is exposed sequentially across sensor columns. In contrast, global shutter sensors expose all pixels simultaneously, a feature preferred in scientific cameras to avoid artifacts. Consumer cameras typically utilize RGB image sensors achieved with a Bayer pattern of color filters over the pixels. Scientific cameras, on the other hand, are usually monochromatic. Additionally, modern consumer cameras often incorporate advanced image processing algorithms that compress and enhance images for aesthetics, making access to raw sensor data rare, yet this is crucial for scientific applications. In this thesis project, a CMOS line sensor was used in the work in Paper VI due to its ability to capture high-frequency wing beats with its high line rate. A CMOS image sensor with good signal-to-noise performance and large pixel size was used in BIOSPACE (Paper I) and the FHSL (Paper II). An InGaAs image sensor was used in the EHSL (Papers III) and SWIR BIOSPACE (Paper IV) due to its SWIR spectral range. The sensors are shown in Figure 4.3 and their spectral ranges are indicated in Figure 4.1.

The number of grey levels ($\#_{\text{grey levels}}$) is an important measure for quantitative measurements. It is determined by the bit-depth of the sensor as $\#_{\text{grey levels}} = 2^{bit\ depth} - 1$, as visualized in Figure 4.3a. The maximum number of charges that can be stored by a pixel is called the full well capacity (FWC) and the dynamic range is the ratio between the highest and lowest signals that can be displayed, calculated by dividing the FWC by N_{read}. In some measurement geometries there is a lot of variation in signal intensity the dynamic range of the camera might not suffice. In these applications, multiple exposures can be stitched together to capture a high dynamic range (HDR) measurement. HDR was used in Paper I to capture both specular reflection and side scattering in the same measurement.

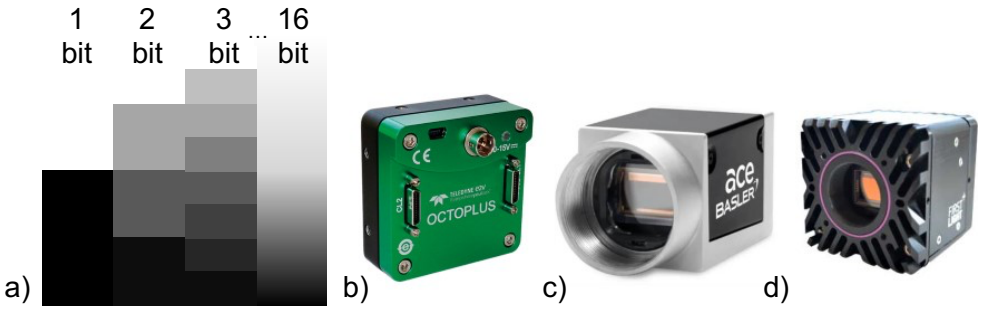

Figure 4.3. a) Visualization of how bit-depth determines the number of grey levels. Common bit-depths of cameras range from 8 to 16 bit. However, cooling is typically required for bit-depths over 12. b) Teledyne Octoplus sensor, was used in the lidar described in Paper VI due to its high line rate of 80 kHz which enables resolving fast wingbeats of different insects. c) Basler ace acA1920-155um used in BIOSPACE and FHSL due to its large pixel sizes. d) First Light C-RED 3 used in EHSL and SWIR BIOSPACE due to it being an InGaAs sensor capable of detecting SWIR wavelengths. Image attributions (b)[vii] (c)[viii] (d)[ix].

4.2.1 Detector noise

In detectors, there is always some degree of random variation mixed with the desired signal, known as noise. Understanding and minimizing noise is crucial for obtaining the most accurate measurements possible. While the signal (S) is proportional to the product of photon flux (Φ), exposure time (t), quantum efficiency (QE), and the system's gain (G), the Signal-to-Noise Ratio (SNR) is a key metric for assessing detector performance, defined as this signal divided by the total noise (N_{total}), *i.e.*, $SNR = S/N_{total}$.

The primary noise sources in imaging detectors can be categorized into Fixed Pattern Noise, Read Noise, Dark Current Noise, and Photon Shot Noise [125].

Fixed Pattern Noise (N_{FPN}) is a static noise inherent to the sensor's characteristics, arising from pixel-to-pixel variations in sensitivity and dark current. These variations are consistent over time and can often be mitigated through dark frame subtraction, especially if the dark level is offset so the variations do not truncate at zero.

Read Noise (N_{read}) originates from random variations in the electronics involved in signal readout, such as the sensor's amplifiers and analog-to-digital conversion circuits. Read noise includes components such as thermal noise, which can increase with the temperature of the electronic components, and flicker noise, which decreases with increased sample frequency (and is therefore also called $1/f$ noise).

Dark Current Noise (N_{dark}) increases with exposure time and is heavily influenced by sensor temperature. It results from the thermal generation of charge carriers within the

sensor even in the absence of light, becoming more significant for long exposures or low-light conditions,

$$N_{dark} \propto \sqrt{t} \tag{4.1}$$

Photon Shot Noise (N_{shot}), is a consequence of the quantum nature of light. The random fluctuations of incoming photons introduce a fundamental noise that is proportional to the square root of the signal strength,

$$N_{shot} \propto \sqrt{S} \tag{4.2}$$

The total noise can be expressed as the square root of the sum of the squares of these noise components, *i.e.*,

$$SNR = \frac{S}{\sqrt{{N_{FPN}}^2 + {N_{read}}^2 + {N_{dark}}^2 + {N_{shot}}^2}} \tag{4.3}$$

Given the proportionalities of the noise sources, the SNR can be described as varying with signal strength and exposure time, not accounting for their temperature and frequency dependence,

$$SNR \propto \frac{S}{\sqrt{C + t + S}} \tag{4.4}$$

where C represents the combined effects of N_{FPN} and N_{read}, t encapsulates the exposure time's influence on N_{dark}, and S reflects the signal strength's impact on N_{shot}.

Different operational conditions can lead to certain noise sources becoming dominant, defining the detector's noise-limited regimes. In high-light conditions (high S), the system often becomes shot noise limited; in low-light conditions, it may become read noise limited; under high temperatures or long exposure times (high t), it can become dark current limited. Understanding these regimes is crucial for optimizing detector performance to ensure the most favorable operational conditions for specific applications [125, 126].

Various methods can be employed to enhance the SNR, including applying analog gain, performing time averaging, utilizing pixel binning, and cooling the sensor. These strategies have been utilized to achieve remote daytime fluorescence measurements of insects with satisfactory SNR. As demonstrated in Paper II, an SNR greater than 150 was achieved for daytime fluorescence observations of tagged honeybees at 18 meters.

4.3 Multi-dimensional cameras

BIOSPACE (Paper I), is a multidimensional camera that expands beyond the two spatial dimensions captured by typical cameras. Here's a breakdown of its six dimensions of light measurement capabilities:

- Dimensions 1, 2, and 3: Spatial Imaging and Morphology: BIOSPACE functions as a camera and incorporates sample rotation to capture three-dimensional structural information.
- Dimension 4: Expanded Spectral Range: Through LED multiplexing, BIOSPACE can analyze a wider range of wavelengths than traditional color cameras.
- Dimension 5: Polarization Sensitivity: Rotating polarization filters allow BIOSPACE to extract valuable information about light polarization.
- Dimension 6: Scattering Angle Analysis: The ability to rotate the light source provides insights into light scattering patterns at different angles.

These capabilities make BIOSPACE a powerful tool for scientific investigation. In the following sections, these measurement domains will be explored.

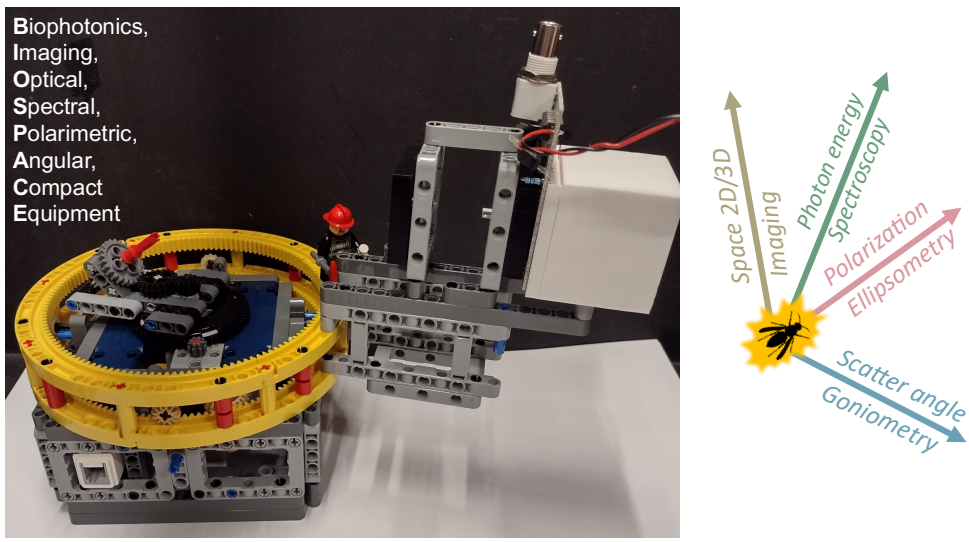

Figure 4.4. Photo of BIOSPACE (left) and the domains it can measure (right). Image attribution [x].

4.3.1 Imaging systems

The subjects of the earliest known photographic attempts, intriguingly, are closely related to the focus of this thesis: leaves and insect wings. In the 1790s, Thomas Wedgwood experimented with capturing these objects using a Camera Obscura and photosensitive silver nitrate [127]. Over the centuries, camera technology has seen significant advancements. Two fundamental milestones that constitute all modern cameras were the transition from a pinhole to a lens, allowing more light to be captured, and the transition from film to digital sensors.

Imaging resolution

The spatial resolution of imaging in two dimensions is determined by both the lens and the sensor. The image of a point source created by a lens manifests as an Airy pattern, which has an angular radius defined by the Rayleigh criterion, which with small angle approximation gives the theoretical lens resolution,

$$r_{Rayleigh} = 1.22\frac{\lambda s}{D} \tag{4.5}$$

where λ is the wavelength, s is the distance between the lens and the sample, and D is the diameter of the lens. This is the diffraction-limited resolution and does not account for lens quality and aberrations.

A more realistic measure is the point spread function (PSF), which describes an imaging system's response to a point source. The image is made by a 2D convolution of the PSF with the object. Quantifying the PSF involves measuring the Full Width Half Maximum (FWHM), which varies with distance along the optical axis, across the image field, and with different wavelengths [128].

The sensor's resolution (ℓ_{sensor}) is determined by the distance between two adjacent pixel footprints at the object plane. This is determined by the magnification (M) of the imaging system and the pixel pitch (ℓ_{pixel}), *i.e.*, the distance between two adjacent pixels in the sensor,

$$\ell_{pixel} = M\ell_{sensor} \tag{4.6}$$

The effective camera resolution is the resolution of the optics sampled by the sensor resolution ℓ_{sensor}. According to the Nyquist-Shannon sampling theorem, sampling at less than twice the spatial frequency of the lens resolution can result in aliasing. Therefore, depending on the sensor resolution, using a lens with higher resolving power could paradoxically lead to a poorer quality image. In Paper I the resolution of the imaging lens was characterized using a Siemens star, a striped pattern with increasingly narrow lines to its center.

Imaging calibration

To acquire a calibrated measurement R_{obj} of an object, typically three images are used: a dark exposure I_{dark}, an image of the reference I_{ref}, and an image of the object I_{obj}. Depending on the measurement geometry R_{obj} represents a measurement of a reflectance transmittance or scattering. The calibrated measurement of the object is determined by,

$$R_{\mathrm{obj}} = \frac{I_{\mathrm{obj}} - I_{\mathrm{dark}}}{I_{\mathrm{ref}} - I_{\mathrm{dark}}} R_{\mathrm{ref}} \qquad 4.7$$

where R_{ref} is the known diffuse reflectance of the reference, known by table values. The reference is typically free of spectral and spatial features. For specular reflectance measurements, a metallic mirror with known reflectance properties can be used as a reference. Alternatively, for forward scattering measurements, an opal diffuser with known Lambertian transmission lobes can serve as an appropriate reference."

4.3.2 3D imaging systems

Various techniques exist to capture spatial information in three dimensions. Our brains achieve 3D vision by processing slightly different images from each eye. Similarly, computer vision algorithms can analyze images from multiple cameras to reconstruct 3D scenes. For this to work, either camera positions must be known or corresponding features in the images must be identified. For stationary objects, 3D information can be obtained by either rotating a single camera around the target or, conversely, rotating the target in front of a stationary camera [129, 130]. BIOSPACE utilizes this latter approach, mounting objects on a LEGO platform and rotating them using LEGO Technic motors (Figure 4.5). However, full 3D reconstruction using BIOSPACE images was not achieved.

A limitation of photogrammetry (like BIOSPACE) is that it only captures the target's surface. For semi-transparent objects, light-sheet microscopy offers a powerful alternative for 3D volumetric imaging [131]. By illuminating the target with a light sheet at different depths, it enables applications like volumetric 3D imaging of embryos [132], and cleared rat brains [133] which would be inaccessible to BIOSPACE.

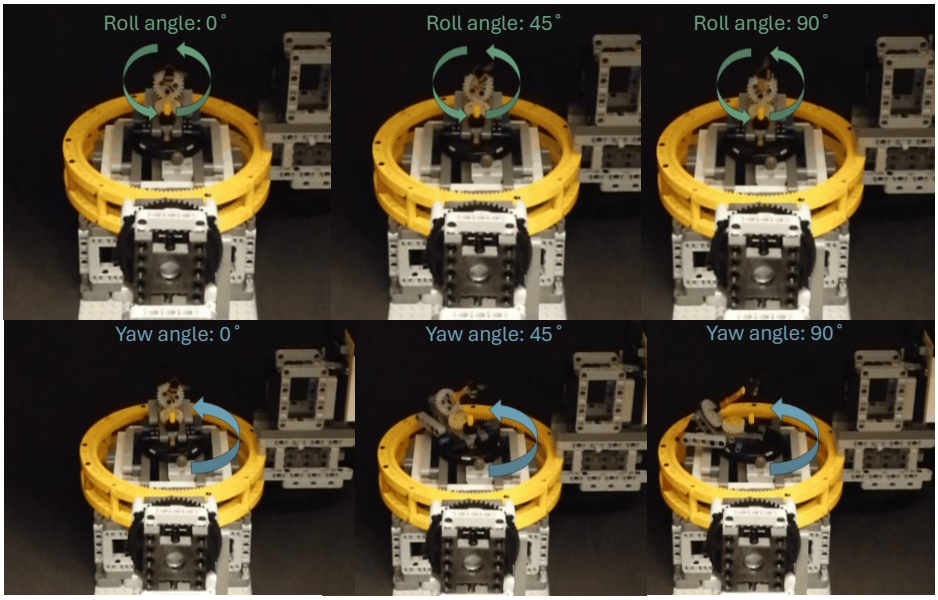

Figure 4.5. The sample rotations enable BIOSPACE to acquire images from all sides of the sample. The top three images show three roll angles of a rotated bumblebee. The bottom three show three yaw angles of the bumblebee. The light source is on the right side while the detector is at the bottom of each image.

4.3.3 Multiplexed multispectral cameras

Resolving different wavelengths of an image can be done either on the detection side or the illumination side. A push-broom hyperspectral camera [134], typically uses a broadband light source and separates the wavelength bands with a grating. What BIOSPACE uses is instead multispectral imaging through time multiplexing. One benefit of multiplexed multispectral cameras is that their spectral range can go beyond an octave, which push-broom systems typically are limited to. The limit on the spectral range for multispectral cameras is determined by the sensitivity of the detector and available light sources.

LED-multiplexing is a commercially viable technique, with applications in diagnosing, *e.g.*, grain [135, 136], meat [119, 137], and blood [138]. The principle is that a multiplexing scheme sequentially illuminates the sample with distinct wavelength bands. Synchronized with each illumination, the detector captures an image, and this process is repeated for all wavelength bands in the system. The multispectral intensity measurement of the object $I_{obj}(b)$ can be expressed as,

$$I_{obj}(b) = \int E_{\lambda_b}(\lambda) R_{obj}(\lambda) S(\lambda) d\lambda \qquad 4.8$$

where $E_{\lambda b}(\lambda)$ is the emitted light in the specific spectral band b, $R_{obj}(\lambda)$ is spectrally dependent reflection of the object, and $S(\lambda)$ is the sensitivity of the system. The $R_{obj}(\lambda)$ can be deduced using a spectrally flat reference and the calibration scheme in Equation 4.7. To ensure positional invariance of the light across wavelength bands, a diffuse cavity can be used. To maximize the dynamic range for all wavelengths, the light sources may be driven at different current levels, reducing intensity variation between the bands. Both a diffuse cavity and intensity equalization were implemented for BIOSPACE and SWIR BIOSPACE with LEDs and LDs respectively. The spectral bands are shown in Figure 4.1. The diffuse white cavity was 3D printed with white ABS plastic which was found to have high scattering and low absorption and fluorescence compared to other 3D-printing materials. A schematic of this implementation is presented in Figure 4.6.

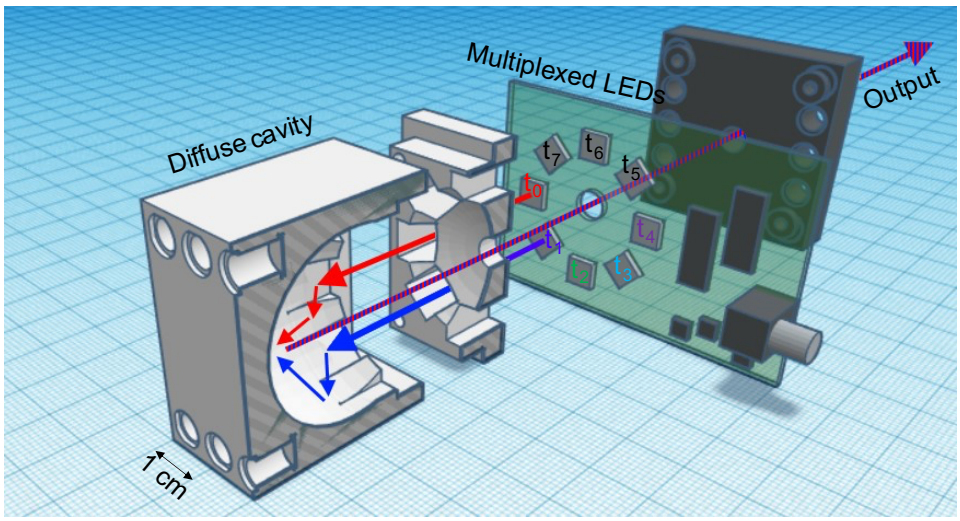

Figure 4.6. LED multiplexing is accomplished by sequentially turning on each LED synchronized with the camera exposures. The diffuse cavity homogenizes the light so the sample is illuminated equivalently for each LED.

4.3.4 Polarization cameras

Polarization imaging can be achieved using a rotatable analyzer placed in front of a detector, capturing the intensity of light at different polarization states. The rotation speed can vary significantly based on the technology: from seconds in mechanical rotators to milliseconds or even nanoseconds with liquid crystal polarizers and Pockels cells. In BIOSPACE, polarization imaging was accomplished using mechanical rotation with low-cost LEGO Mindstorm motors as shown in Figure 4.7.

A recent development in polarization imaging is polarization image sensors [139]. These sensors are equipped with four differently angled linear polarization filters, positioned in front of the pixels. This arrangement is analogous to the color filters in a Bayer pattern used in color cameras. The polarization filters are oriented at 0, 45, 90, and 135 degrees, allowing for the resolution of polarization information in the captured light.

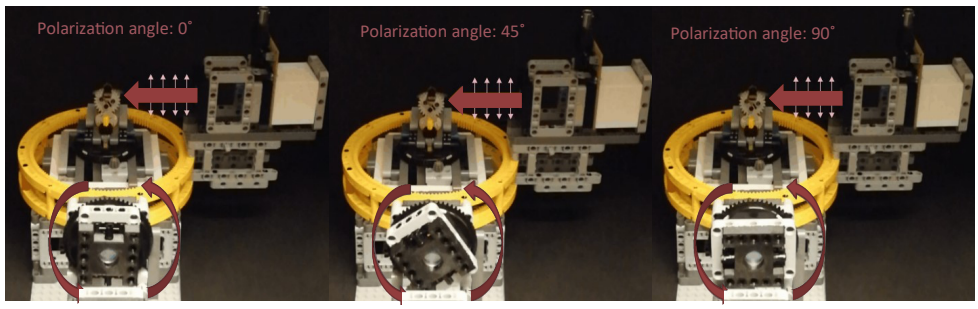

Figure 4.7. The light source is illuminating the sample with polarized light which is probed with a rotating analyzer. The light source (at the right of each image) is emitting polarized light while the analyzer at the bottom is rotated.

4.3.5 Goniometric cameras

Goniometric cameras, or goniometers, are instruments designed to measure light intensities at different angles from a target object. This is typically achieved by rotating a detector around the object to characterize the emission lobes of light sources or to measure the reflected or scattered lobes of investigated materials. The alternative is to rotate the illumination source around the object, which was done for BIOSPACE (Figure 4.8). The resolution of goniometric measurements is limited by the precision of the rotating arm's angular positioning and by the convolution of the imaging lens's field of view and the light source's emission cone.

In satellite remote sensing, goniometers can define bidirectional reflectance distribution function (BRDF) models. These models describe the reflection anisotropy of Earth's surface [140]. In the field of biophotonics, goniometers are used to measure the scattering properties of, *e.g.*, fruits [141], suspended particles [142], and insects [25, 143].

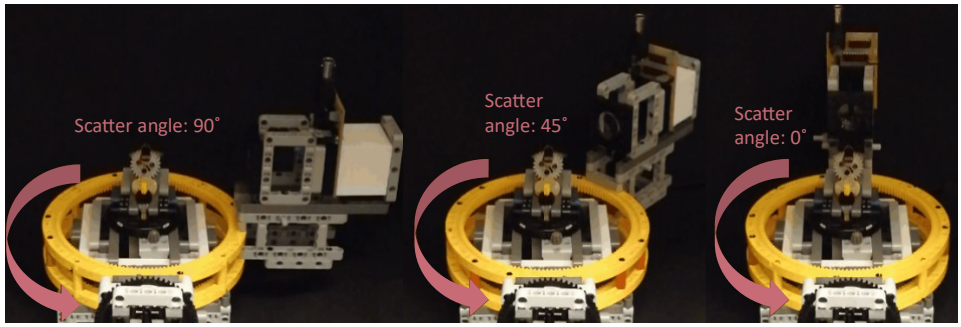

Figure 4.8. Goniometry was accomplished by rotating the light source around the target to different scattering angles.The detector is located at the bottom of each image while the light source is rotated to scattering angles of 90, 45, and 0 ˚

4.4 Lidar

Since the 1960s, the predominant approach to laser ranging has been sending out short pulses and counting the time-of-flight (ToF) [144], or transmitting frequency-modulated continuous waves (FMCW) where the returning frequency chirps are analyzed to find the distance and velocity of targets through the doppler shift [145]. In ToF lidars, the temporal resolution and range limits are limited by the pulse repetition rate, and the range resolution is limited by the pulse width. In FMCW lidar the chirp duration, bandwidth, and repetition frequency determine the temporal and spatial resolution and the ambiguity range. Scheimpflug lidar instead uses triangulation to resolve range onto different pixels on a sensor. Due to the fundamentally different design of the Scheimpflug lidar, range resolution, and range limits are not limited by the pulses or frequency sweeps of the laser. Instead, temporal resolution is limited by the detector's sampling rate. Its spatial resolution depends on the angles used in the Scheimpflug configuration and the detector's pixel sizes and decreases with distance from the system [146, 147].

4.4.1 The Scheimpflug principle

Originating from aerial photography in the early 1900s [148, 149], the Scheimpflug principle, along with the Hinge rule, was a method to tilt the plane of sharp focus. This allowed large areas to be imaged from hot-air balloons and airplanes without increasing the camera's depth of field. Normally, depth of field can be increased by reducing the camera's aperture size, but this limits the light collection, necessitating longer exposure times and potentially causing motion blur (visualized in Figure 4.9). The Scheimpflug principle ensures that an entire object plane is in focus if it intersects with the lens plane and the detector plane at a single point. Additionally, according to the Hinge rule, the front focal plane of the lens and the detector plane, extended to the lens center, must intersect at a single point as well (Figure 4.10).

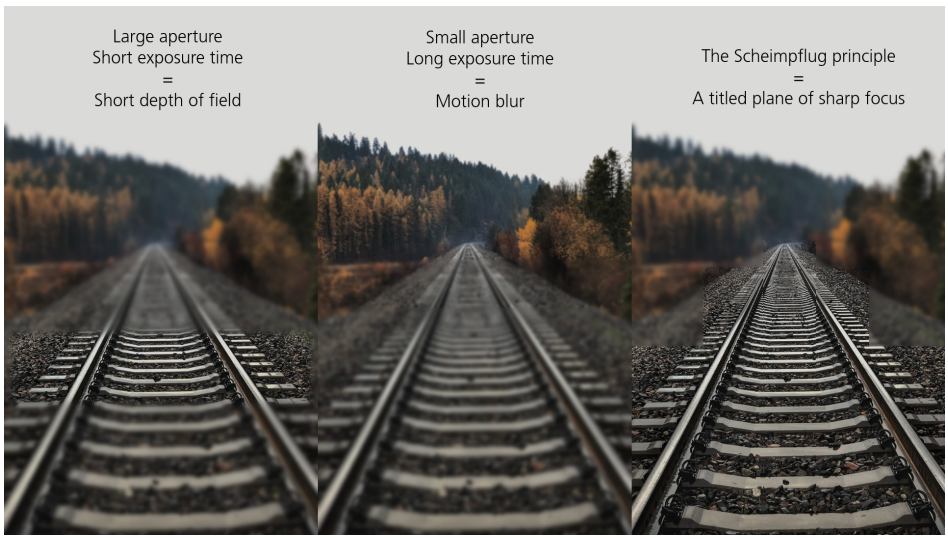

Figure 4.9 Visualization of camera setting tradeoffs and the Scheimpflug principle. (a) A photo taken from a moving train with a large aperture and short exposure time focuses sharply at a specific distance, but results in a limited depth of field, causing blurriness at other distances. (b) Increasing the depth of field with a smaller aperture necessitates longer exposure, leading to motion blur. (c) Employing the Scheimpflug principle to tilt the plane of sharp focus allows for a clear image across the entire train track. Image attribution [xi].

4.4.2 Scheimpflug lidar

Although long known in photography, the Scheimpflug principle was only combined with lidar in the 2010s [41, 146, 150]. It has been applied in studies of atmospheric composition [151-153], combustion [154], entomology [25, 44, 48], and vegetation [155]. In a Scheimpflug lidar system, the laser transect is aligned with the object plane, enabling ranging as the laser light is absent outside this plane. The range r (m) corresponds to a normalized sensor position $p_r \in [0 \ldots 1]$, can be approximated as,

$$r(p_r) = \ell_{BL} \cot(\Phi_{slant} + \Theta_{FoV} p_r) \qquad 4.9$$

where ℓ_{BL} (m) is the baseline length, Φ_{slant} (°) is the slant angle, the angle between the optical axis of the receiving lens and the laser transect, and Θ_{FoV} (°) is the receiver field of view, as seen in Figure 4.10. A detailed discussion on ranging with Scheimpflug lidar is found in [156].

The size of an object detected by a Scheimpflug lidar can be approximated in two ways, called optical cross section and apparent size. None of these measurements have higher than single-digit precision but indicate the size of the target. The optical cross is related to the intensity of the backscattered signal, which can be calibrated for different ranges by measuring a target of known reflectance and size and the backscattered intensity from the air along the transect. The apparent size instead relates to how many range pixels the observed target is registered in. A detailed discussion on sizing is found in [157].

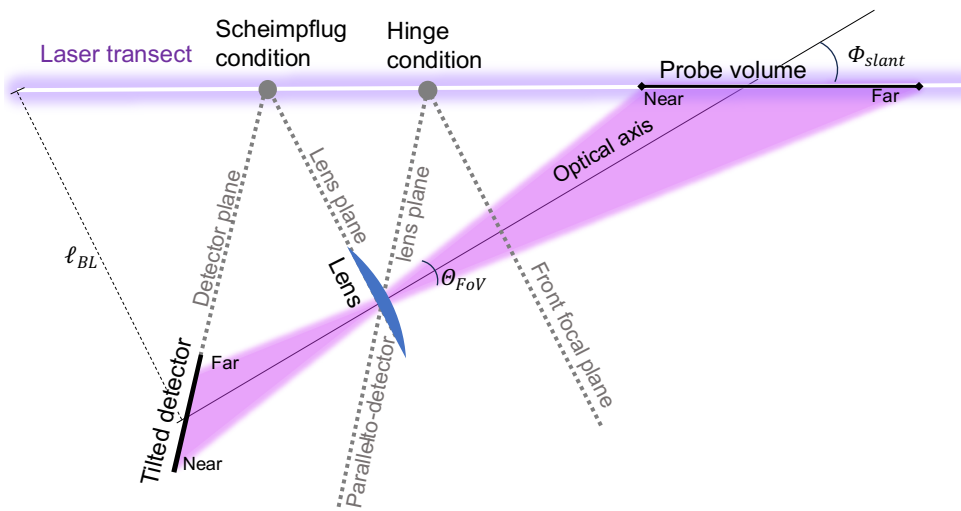

Figure 4.10. Visualization of the Scheimpflug and hinge conditions in a Scheimpflug lidar setup. The different pixels of the tilted detector correspond to different distances from the lidar. The distances and angles in the image are exaggerated for clarity.

Figure 4.11. Andrew, Rabbi, and Adolphe are aligning the Scheimpflug lidar in a virgin rainforest in Côte d'Ivoire for measuring insect biodiversity (Paper VI). Left to right on the baseline there is mounted a receiving Newton telescope, a laser driver box, a monitor camera telescope, and a laser expander with two laser diodes.

Scheimpflug lidar can incorporate multiplexed lasers for acquiring different wavelengths [158, 159], polarizations [160], and for implementing background subtraction [44, 161]. In this thesis project, a Scheimpflug lidar system with multiplexed polarization was utilized to measure insect biodiversity in a virgin rainforest in Côte d'Ivoire (Paper VI, Figure 4.11). Background subtraction was implemented through time multiplexing in the FHSL (Paper II, V, VII-IX) which made daytime fluorescence measurements possible, despite the background signal having higher intensity than the recorded fluorescence signals.

4.4.3 Hyperspectral Scheimpflug lidar

The Scheimpflug lidar was expanded to a hyperspectral Scheimpflug lidar (HSL) in the 2010s for studying fluorescence from aquatic fauna [162-164] and vegetation [155]. This was accomplished by building upon the design principles of the Scheimpflug lidar depicted in Figure 4.10. Here, the detector is replaced with a slit, which is then dispersed and imaged onto an area detector. Due to the tilt of the slit relative to the optical axis, a second set of Scheimpflug and hinge conditions must be fulfilled, as illustrated in Figure 4.12.

In this thesis, two HSLs were designed, the FHSL for fluorescence applications in the visible spectrum (Paper II, Figure 4.13, Figure 4.14b) and the EHSL for elastic

measurements in the SWIR region (Paper III). Since the field is relatively young, these papers presented the first entomological HSL measurements using both fluorescent and elastic light.

The data captured by the detector of an HSL has range along one axis and wavelength along the other. By combining multiple exposures, the information can be organized into a tensor with range, time, and photon energy for further processing, see Figure 4.14a. However, due to optical distortions, the wavelength and range axes are not entirely independent. The wavelength at each point can be approximated by normalized detector positions p_r and p_λ on a polynomial plane,

$$\hat{\lambda}(p_r, p_\lambda) = \lambda_0 + \lambda_{span} p_\lambda + \delta_{fan} p_\lambda p_r + \delta_{bend} {p_r}^2 \qquad 4.10$$

where λ_0 (nm) represents the shortest wavelength detected by the lidar, and λ_{span} (nm) denotes the total wavelength span. The coefficients, δ_{fan}, and δ_{bend} account for 'keystone' and 'smile' artifacts [134, 165] which impact spectral registration at different ranges. See Paper III for a detailed discussion on spectral calibration of HSLs.

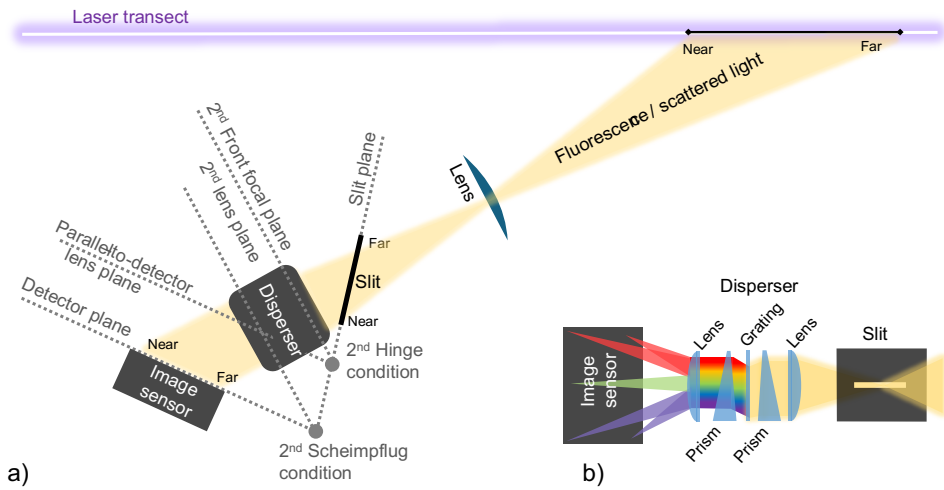

Figure 4.12. a) Visualization of the second set of Scheimpflug and hinge conditions in a hyperspectral lidar. b) The spectral view is rotated 90˚ compared to a). The received light is dispersed onto a 2D image sensor with a collection of optical elements such that one dimension of the image sensor corresponds to range and the other to wavelength.

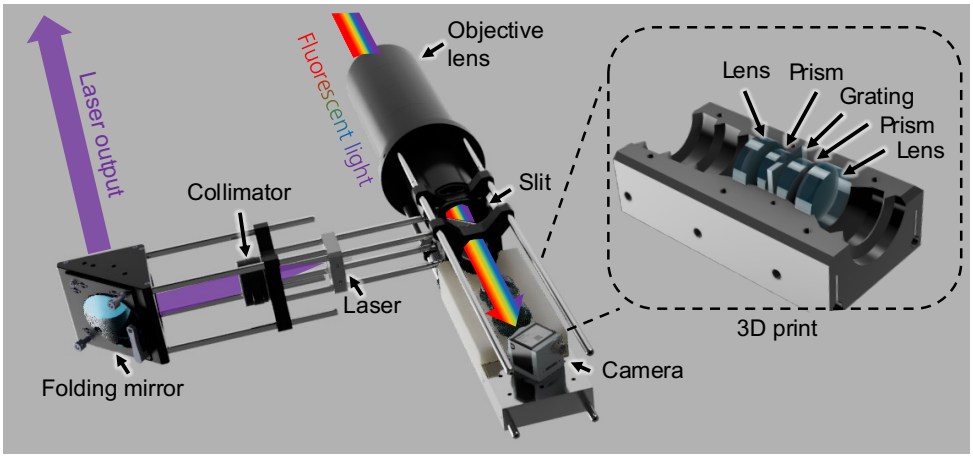

Figure 4.13. Schematic of the FHSL. The laser light is collimated and folded, and the fluorescent signal is imaged with the objective lens onto a slit after which it is dispersed and imaged onto the camera detector.

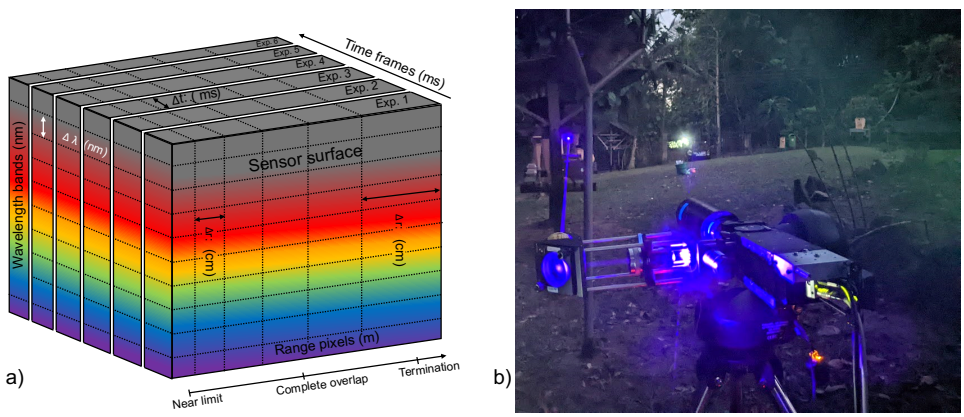

Figure 4.14. a) The data acquired by a HSL has range and wavelength information on the pixels of the sensor, and time information with the exposure numbers, forming a data cube. b) The FHSL measuring activity of stingless bees at the International Stingless Bee Center in Ghana (Paper V).

5 Design of optical instrumentation

The design of an optical system requires careful consideration of several factors. Key objectives include defining the desired resolution in terms of wavelength, time, and space, along with the target wavelength range. Practical constraints like eye safety, cost, portability, reproducibility, and anticipated operating conditions (light levels) must also be addressed. Finally, ensuring an acceptable signal-to-noise ratio (SNR) through a balance of component choices and measurement parameters is crucial.

Since BIOSPACE measures stationary objects, high frame rates were not a priority. Instead, SNR could be improved by increasing exposure times, as long as no spectral band is saturated. Prioritizing LED current adjustment was therefore important to achieve a balanced emission spectrum. To measure interesting phenomena outside of the visible spectrum such as hemoglobin and water absorption peaks, the spectral range was maximized from UV to NIR, based on available LEDs and limits from camera sensitivity.

For the FHSL a high frame rate is needed to measure insects in flight. However, the frame rate is ultimately balanced with SNR for sufficient signal strength. The 100m measurement distance necessitated a highly sensitive sensor (with large pixels) and a powerful laser. Given the spectrally broad fluorescence of both plants and tagging powders, the focus was on capturing a wide spectral range rather than maximizing spectral resolution.

Both BIOSPACE and the FHSL emphasized low cost, compact size, and ease of replication for accessibility and broader scientific impact.

5.1 Ray tracing

Ray tracing, using the paraxial approximation, provides a valuable tool for the initial design of imaging and lidar systems. The thin lens equation is often sufficient for this stage:

$$\frac{1}{f} = \frac{1}{s} + \frac{1}{s'} \tag{5.1}$$

where f is the lens focal length, s is the object distance, and s' is the image distance. During initial design, components are typically treated as 'ideal' without aberrations or dispersion effects. Dispersion, where focal length varies with wavelength, causes

chromatic aberrations in lenses. This is problematic for spectroscopy and mitigated using mirrors or achromatic lens combinations. Achromats combine materials with different dispersion properties, minimizing focal length variation over a desired spectral range. Such lenses were used in the spectroscopic designs of BIOSPACE, FHSL, and EHSL.

Diffraction, the bending of waves around obstacles or through apertures, sets the fundamental resolution limit for imaging systems. It also underpins the function of diffraction gratings, used to separate wavelengths. Gratings with periodic surface structures produce intensity maxima at specific angles:

$$d(\sin\theta_m \pm \sin\theta_i) = m\lambda \qquad 5.2$$

Where λ is the wavelength, d the grating spacing, θ_i the incidence angle, θ_m the diffraction angle, and m the diffraction order. Blazed gratings, optimized for a specific wavelength and diffraction order, were used in the FHSL and EHSL.

Ray tracing software enables fine-tuning of component placement and resolution calculations. It incorporates extensive libraries of lenses, materials, and coatings. This detailed information, coupled with computational power, makes it possible to optimize systems through iterative ray tracing, to minimize aberrations and artifacts. The geometric optics approximation was sufficient for BIOSPACE. However, ray tracing software played a crucial role in developing the FHSL and EHSL (Figure 5.1).

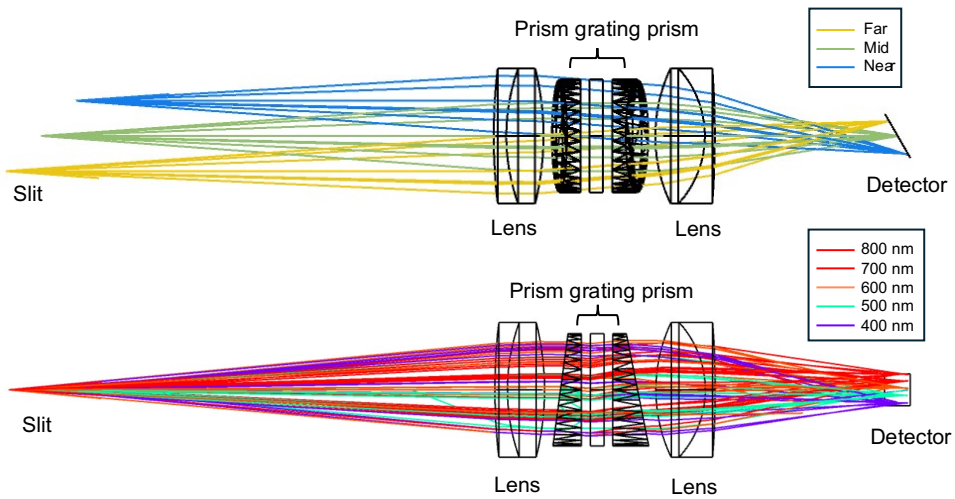

Figure 5.1. Ray tracing of FHSL from Zemax. The top view shows rays from different positions along the slit, giving range information. The bottom view shows rays of different wavelengths, giving spectral information.

5.2 Mechanics

To bring an optical design from a sketch to a physical model, a mechanical structure is needed. Optical systems in laboratory environments are often mounted in cage or tube systems. These setups require manual tuning and calibration to achieve specific distances and angles. While cage systems allow for high precision, replicating the exact angles and distances optimized through ray tracing software can be challenging. This is where computer-aided design (CAD) software becomes advantageous. The precise locations of optical components, as determined by ray tracing, can be exported to CAD software. Here, supporting mechanics can be designed with appropriate slots for components and baffles to reduce stray light. Such designs can be brought to life using 3D printing for plastic components [166-168]. For parts requiring metal, such as heatsinks, computer numerical control (CNC) milling of aluminum is often preferred, though metal 3D printing is an option.

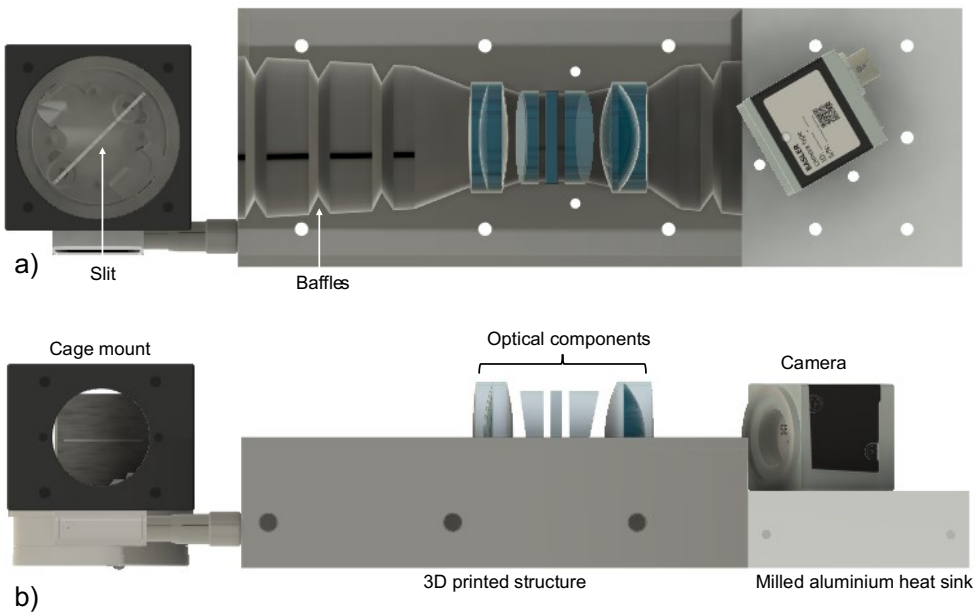

Figure 5.2. The mechanical structure of the FHSL is a combination of cage mounts 3D printed plastics and CNC milled aluminum for mounting the camera. The positions of all elements are based on raytracing optimizations and the views in a) and b) correspond to those shown in Figure 5.1a and b.

In this thesis work, a combination of optical cage systems, ray tracing-optimized 3D-printed plastic, and CNC-milled aluminum parts were utilized in the design of FHSL (Figure 5.2) and EHSL. For BIOSPACE, a low-cost, modular, and adaptable design was prioritized. Therefore, 3D-printed plastic was merged with LEGO® Technic™ high-precision modular plastic building blocks to provide the mechanics for the designs (Figure 4.4).

5.3 System control and data acquisition

With optics and mechanics in place, the acquisition and light sources need to be controlled. Image sensors are often equipped with hardware for connection to laptops or microcomputers via USB, GigE, or Camera Link interfaces. In contrast, while turn-key lighting systems exist for specific applications [137], custom designs often require assembling individual components such as laser diodes (LDs) and LEDs, along with their respective driving circuits. Both LDs and LEDs require constant current operation, as the power-voltage ratio increases with temperature, making constant voltage operation unsuitable. Laser diodes and LEDs have rise and fall times in the order of tens of picoseconds and tens of nanoseconds, respectively [169, 170]. This fast response time allows for multiplexing schemes for multiple wavelengths, polarizations, and background subtraction. In this thesis project, a multiplexed LED driver was implemented for BIOSPACE, while multiplexed laser drivers were developed for FHSL and SWIR BIOSPACE. The BIOSPACE drivers (Papers I and IV) were built on custom-made printed circuit boards (PCBs), created using a CNC router (Figure 5.3).

Acquisition software needs to be tailored for the optical system. In this thesis work, acquisition software has been developed in Python (Paper I), and in LabVIEW (Paper II, III, and VI). These programs have been made open source and are available on GitHub [82-86]. While LabVIEW programs can be run freely, any code modifications require a commercial license.

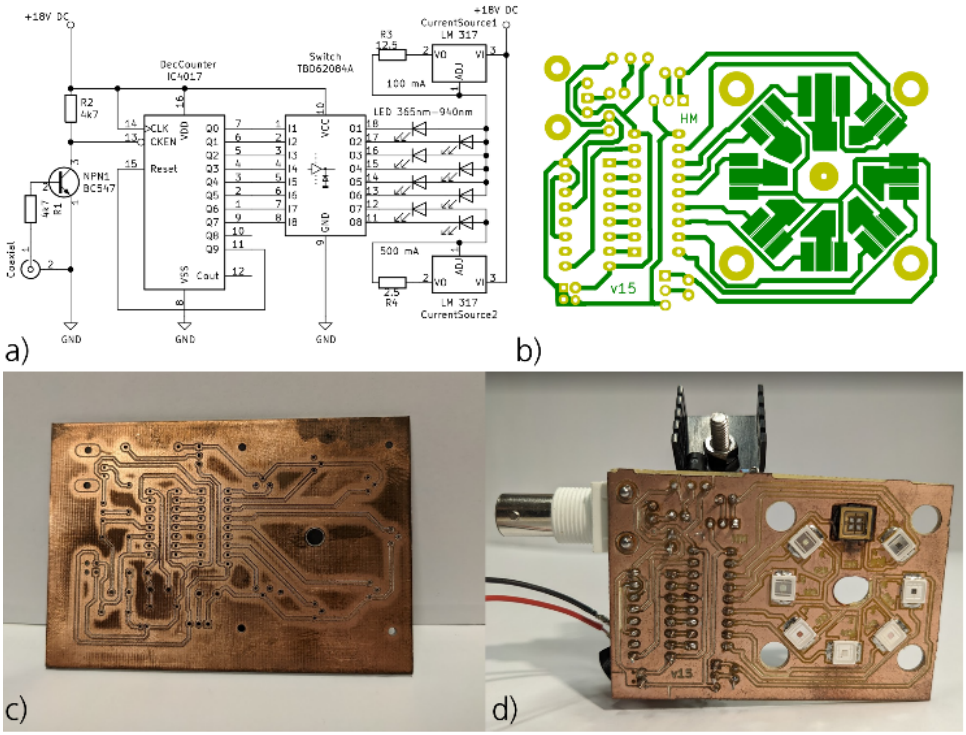

Figure 5.3. a) Circuit diagram of LED multiplexing printed circuit board (PCB) for BIOSPACE. It consists of a coaxial input, a decade counter, a transistor array, two constant current sources, and eight LEDs. b) The PCB layout, in green are tracks to connect components and yellow circles are drill holes for through-hole components. c) The routed PCB without mounted components. d) The light source with all components soldered, the LEDs are surface mounted all other components are through hole.

6 Data processing

"Data is the new oil. It's valuable, but if unrefined it cannot really be used".

- Clive Humby, 2006

Raw data typically needs processing to be useful. The data handled in this thesis can be divided into two categories: Multidimensional imaging data from BIOSPACE and SWIR BIOSPACE, and sparse lidar data from the multiplexed and hyperspectral lidars. These datasets need processing with different methods to extract relevant information. Such methods which were used in this thesis work will be described below.

6.1 Multidimensional imaging data

BIOSPACE produces $I(x, y, b, scatter, roll, yaw, pol)$, a 7-dimensional intensity tensor, where the integer indices correspond to the following vectors. Spatial imaging information is encoded in ℓ_x, ℓ_y [mm]. Spectroscopy data is found in λ_b [nm], denoting the LED wavelength bands. Goniometry is represented by $\theta_{scatter}$ [°], which indicates the angle of the light source. Sample orientation in 3D is described by θ_{roll} and θ_{yaw} [°], while θ_{pol} [°] describes the polarization state of the light. To visualize all this information one can, *e.g.*, utilize plots, 2D heatmaps, or false color representations. However, it is not possible to visualize the full measurement in one representation, instead, each visualization focuses on one or two dimensions, as illustrated in Figure 6.1. Different models of absorption or scattering can be fitted to the spectra or phase functions measured to deduce specific optical properties of the samples such as the scattering coefficient of blood, as discussed in Paper I, and water and melanin pathlengths, as described in Paper IV.

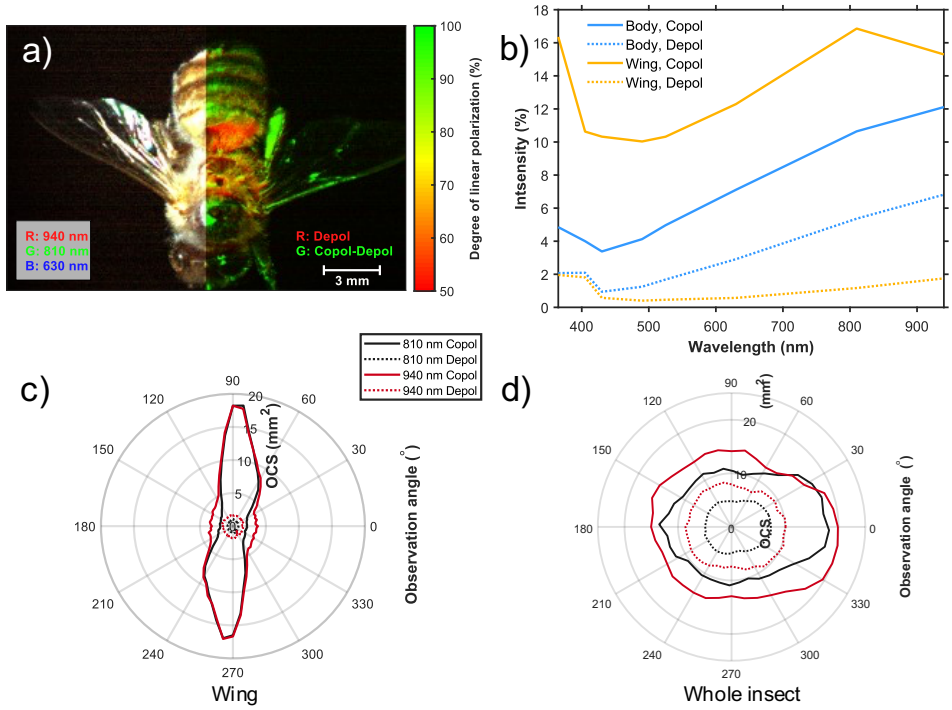

Figure 6.1. A multidimensional measurement, visualized in multiple ways. a) Two false-color images, to the left, based on near-infrared wavelengths, and to the right the degree of linear polarization is visualized by having the red color channel showing the intensity of depolarized light, while green is displaying the difference in intensity between copolarized and depolarized light. b) Spectra of the sample for the body and the wing and the two polarizations. The lower polar plots show intensity depending on the observation angle for c) the insect wings, and d) the whole insect.

6.2 Hyperspectral Scheimpflug lidar data

6.2.1 Insect observation extraction

Entomological lidar data mainly consists of background signals, with occasional higher-intensity signals indicating insects crossing the laser beam. Efficient processing requires extracting these insect observations for further analysis.

In FHSL measurements, an insect observation exhibits an intensity peak due to elastic scattering. When tagged with fluorescent powder, an additional peak appears at the corresponding fluorescence wavelength. To detect observations, all ranges are evaluated. If an intensity peak exceeding a suitable threshold occurs at both the elastic

wavelength and its second-order harmonic, an insect is detected. Figure 6.2 illustrates processed data, highlighting three elastic and two fluorescent observations.

Based on the distribution of recorded light intensities, a statistically derived threshold can optimize detection. A thorough data processing pipeline is presented in Paper V.

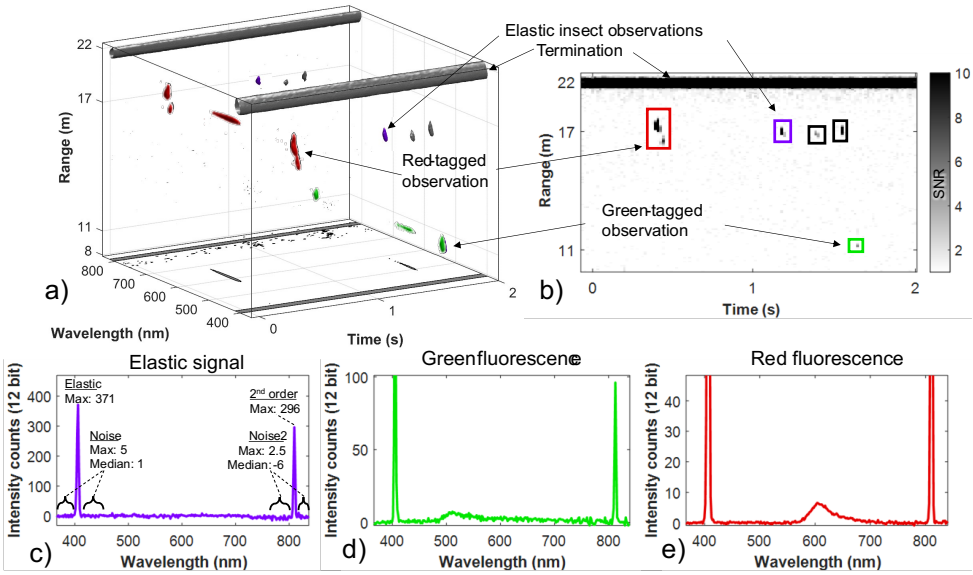

Figure 6.2. Data processing of an FHSL measurement file. a) Five insect observations and the termination echo are visible. Three observations are highlighted: untagged (violet), green-tagged (green), and red-tagged (red). Projections onto the wavelength-time plane are in black. b) Signal-to-noise ratio (SNR) at each range-time element. The SNR was defined as the elastic peak compared to the noise level (detailed in Paper V). c) Selected insect spectra (colors correspond to a). Values used in SNR calculations (Eq. 1, Eq. 2) are shown.

6.2.2 Vegetation scanning

The fluorescence spectra contained within FHSL lidar echoes offer valuable information for analysis. In the work presented in Paper VII, we employed singular value decomposition (SVD) for differentiating tree species (Figure 6.3). SVD decomposes spectra into a set of eigenvectors and corresponding eigenvalues (representing their significance). By focusing on the most significant eigenvectors, we can reconstruct the original spectra with reduced noise. This facilitates robust comparisons using techniques like hierarchical clustering analysis (HCA).

By scanning the lidar in a raster pattern, with a motorized tripod, each exposure number corresponds to specific azimuth and altitude angles. Since the lidar captures range information, we have all the information needed for recreating a point cloud. This was done for a forest edge, coloring the points based on the fluorescence spectra (Figure 6.3e). For further details on vegetation fluorescence analysis, see Papers VII and VIII.

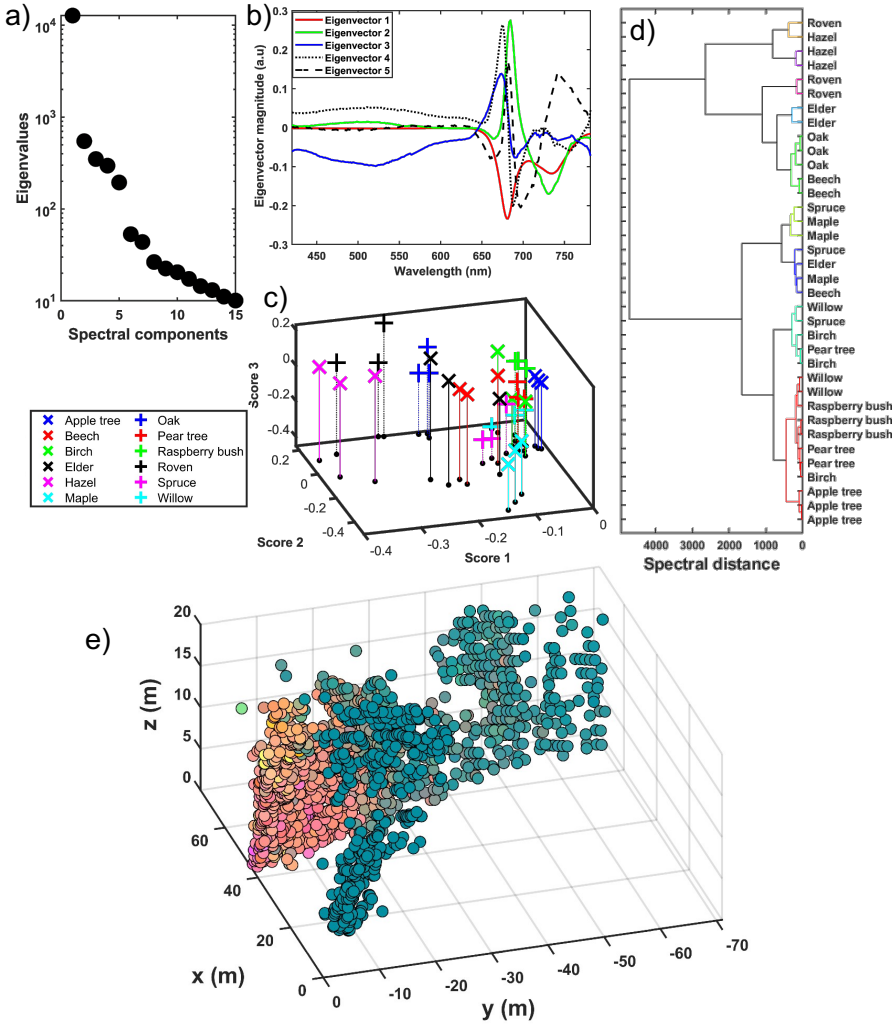

Figure 6.3. Singular value decomposition of fluorescence spectra from leaves of different species. a) shows the eigenvalues, b) the first five eigenvectors, and c) the first three scores of the different species. d) Hierarchical clustering analysis of the different species. e) A point cloud of a forest edge, where the colors of the points are determined by the first three eigenvector scores.

7 Conclusion

This thesis presents the development and implementation of innovative biophotonic instruments, distinguished by their novelty, versatility, and accessibility. This includes the first remote real-time full-waveform laser-induced fluorescence spectrum during full daylight of both insects and vegetation, the first lidar with 70 spectral bands, and the first remote wing-thickness measurement of insects in flight with lidar. The designs prioritize open-source principles, low cost, modularity, and field readiness. Reproducibility have been demonstrated through international workshops, where components, LEGO® sets and a and a 3D printer was brought for onsite assembly. Instruments were successfully deployed across multiple countries (Sweden, Ghana, Côte d'Ivoire, and France). Furthermore, their value in education is proven through project-based learning activities at Lund University, benefiting over 50 students to date.

Low-cost, accessible scientific tools are crucial for advancing biophotonics and remote sensing – fields key to understanding insect behavior, vegetation health, and disease spread. By making these tools widely available, we pave the way for greater insights into biodiversity, plant stress detection, and targeted pest management. These insights benefit agriculture, ecology, and public health.

Today entomological lidars from our group in Lund are spread across the globe (Figure 7.1). While this thesis project emphasized technology, it also sets the stage for the next phase of research. Going from here, I wish for continued advancement, strategic planning, and insightful analysis of nature. The focus can shift towards large-scale, carefully designed experiments that utilize this technology to give answers to important biological questions. Answers that have the potential to inform policy decisions and strategies for malaria prevention, biodiversity conservation, and sustainable agriculture. Our instruments have proven their value – now let's use them to expand scientific understanding for positive change.

Figure 7.1. A world map of Scheimpflug lidars for biophotonic remote sensing.

Acknowledgments

Some say PhD stands for *permanent head damage*; while that can certainly be true, it can also be a journey full of new experiences, perspectives, and friendships.

I would like to start by thanking my supervisor Mikkel Brydegaard. When I first contacted you about a crazy jungle physics PhD position, I got an autoreply that you were in the wilderness without internet. From that moment I knew this would be an adventure. I'm grateful to have had you as my supervisor. Your combination of theoretical knowledge and hands-on skills is unmatched and you are always willing to share your time and knowledge. You are truly keeping science funky.

Joakim Bood and Aboma Merdasa, I'm very happy to have had you both as my co-supervisors. You are both kind and sympathetic and its always easy discussing things with you. Joakim you are a voice of reason at the division and fit perfectly for your new role as head of division. Aboma, I admire your passion, it's a shame we had to cancel our Ghana-trip due to that annoying pandemic, it would've been fun!

Meng Li, my companion on this journey, you are so kind, supporting, and brilliant. I've enjoyed all our field trips even though I know you prefer Staffanstorp with Karl and Ace over hammocks in the jungle. We've been through so much together, from freezing nights in sleeping bags, avoiding forest fires, and taxi drivers ripping us off - and worst of all - those damn green bags. You always keep me up to date with the latest gossip and make sure there are some Chinese sweets on my table. thank you for everything! Lauro Müller, it has been so great to work with you, you are smart kind and full of energy. I honestly have no idea how you always manage to squeeze in a 5-hour surfing session whenever there are waves somewhere within driving distance. I hope you will be back in Lund as often as possible, for some fisksoppa, some great coffee at Göteborgs, or playing some volleyball in our matching "cent pourcent d'Ivoirienne" T-shirts. Samuel, thank you for your warm welcome into the group. You showed that it's possible to be extremely productive and to have fun in the process. Playing Heroes in Nyteboda will remain a fond memory. Let's continue catching up over some disc golf. Everyone in our group, Klas, Jacobo, Isa, Zhicheng, Dolores, David, and Emanuell, thank you for all the interesting and fun discussions during our group meetings, it's been a blast.

To my African friends, Andrew, Rabbi, Doria, and Adolphe: it has been so much fun to work with you in our own little team. You are all so kind and driven, it will be a joy to follow your paths in the future and I hope to see you many times again. Andrew, thank you for showing me all different types of meals Ghana has to offer, thank you for having clothes sewn for me and Josefin! Rabbi, thank you for the Ghanese traditional hat. I will always remember the hesitant swimming lessons fondly. Doria and Adolphe, thanks for putting

up with my poor French with patience and smiles and thank you for cooking those amazing meals in the jungle.

Thank you, Benjamin Anderson, Jeremie Zoueu, and Carla Puglia of AFSIN and ISP for making the research trips possible. And to all AFSIN members, Benoit, Peter, Charles, Konin, and colleagues. Thank you for your hospitality, it's been such amazing journeys for me thanks to you all.

Thank you, Tidiane, our stable point in an otherwise wild jungle experience. Your help and kindness extended far beyond being our driver. GTA, thank you for saving us from the tarantula in the house, you took your job guarding us seriously while finding some time to watch all those dubbed Tom Cruise movies in the evenings. Thank you, Sam, for hosting me at the Stingless Bee Center and showing me your home village, it's a special memory.

Thank you, Rickard and Mengistu, for breeding mosquitoes for my experiments and taking time teaching me how to handle them. Being able to see the difference between male and female mosquitoes is one of my weirder party tricks. Thank you, Carsten, for your help and friendliness during our lidar campaigns. Thank you Malin Malmsjö for hosting me in your laboratory, and Nina Reistad for your help and lending me equipment.

Bernd, Serge, Willy, and Camille, thank you for hosting me in Paris, you're passionate and easy to work with while still finding the time to enjoy some great food in French proportions.

To everyone at the division. David Frantz, Adrian, Henrik, David Sanned, Vassily, David Andersson, Lisa, Simon, Meena, Aravind, Martin, Jonas, Sebastian, Yupan, Saga, Marco, Yue, Jundie, Saeed, Armand, Sabrina, Jefry, Megha, Giota, Zhiyong, Kailun, Alsu, Ruike, Dina, Panagiota, Alexios, Sabrina, Emma, Robin, Lovisa, Frej, Carl, August, Marcus, Per-Erik, Sven-Inge, Christian, Eduard, Andreas, Elna, Elias, Cuong, Erik, Vladimir, Ruan, Arman, Göran, Johan, Ali, Niklas, Alexander, Adam, Li, Frederik, Pontus, Anna-Lena, Moa, Jinguo, Birgitta, Carlton, Igor, Minna, Cecilia, Emelie and Charlotta. Thank you for all the fun discussions in the corridors, all the fika, discgolf excursions, badminton, brännboll, and movie nights. The atmosphere is great at the division and its thanks to all of you.

Finally, I would like to thank my friends and family for all your love and support. I'm truly blessed with such great friends, and extended family, I can't list you all, but you know who you are. Please take pride in knowing you are the best and mean so much to me! To Mom, Dad, Jesper and Fanny, thank you for inspiring me to always be curious about the world, and for providing the stability that has allowed me to go on all my adventures. It's not something often said but I am incredibly proud to have you as my parents and siblings and I love you very much. Josefin, my marvelous wife and love of my life, words cannot describe how much you mean to me. I'm so grateful to share my life and all adventures, big and small, past and future, with you.

This work does could not be accomplished without you all. And even if it only amounts a drop in an ocean: to return to quote at the beginning of this thesis – *what is an ocean but a multitude of drops.*

References

1. Ellis, H., *A history of surgery*. 2002: Cambridge University Press.
2. Manktelow, M., *History of taxonomy*. Lecture from Dept. of Systematic Biology, Uppsala University, 2010. **29**.
3. Bar-On, Y.M., R. Phillips, and R. Milo, *The biomass distribution on Earth*. Proceedings of the National Academy of Sciences, 2018. **115**(25): p. 6506-6511.
4. Klowden, M.J., *Physiological systems in insects*. 2013: Academic press.
5. Ollerton, J., *Pollinator diversity: distribution, ecological function, and conservation*. Annual review of ecology, evolution, and systematics, 2017. **48**: p. 353-376.
6. Michener, C.D., *The bees of the world*. Vol. 1. 2000: JHU press.
7. Grüter, C., *Stingless bees*. Cham, Switzerland: Springer International Publishing, 2020. **109**(4): p. 1182-1186.
8. Potts, S.G., et al., *Global pollinator declines: trends, impacts and drivers*. Trends in ecology & evolution, 2010. **25**(6): p. 345-353.
9. Potts, S.G., et al., *Declines of managed honey bees and beekeepers in Europe*. Journal of apicultural research, 2010. **49**(1): p. 15-22.
10. Chuttong, B., Y. Chanbang, and M. Burgett, *Meliponiculture: Stingless bee beekeeping in Thailand*. Bee world, 2014. **91**(2): p. 41-45.
11. Toledo-Hernández, E., et al., *The stingless bees (Hymenoptera: Apidae: Meliponini): a review of the current threats to their survival*. Apidologie, 2022. **53**(1): p. 8.
12. Tornyie, F. and P.K. Kwapong, *Nesting ecology of stingless bees and potential threats to their survival within selected landscapes in the northern Volta region of Ghana*. African Journal of Ecology, 2015. **53**(4): p. 398-405.
13. Das, A.J., N.L. Stephenson, and K.P. Davis, *Why do trees die? Characterizing the drivers of background tree mortality*. Ecology, 2016. **97**(10): p. 2616-2627.
14. Oliveira, C., et al., *Crop losses and the economic impact of insect pests on Brazilian agriculture*. Crop Protection, 2014. **56**: p. 50-54.
15. Christiansen, E. and A. Bakke, *The spruce bark beetle of Eurasia*, in *Dynamics of forest insect populations: patterns, causes, implications*. 1988, Springer. p. 479-503.
16. Komonen, A., L. Schroeder, and J. Weslien, *Ips typographus population development after a severe storm in a nature reserve in southern Sweden*. Journal of Applied Entomology, 2011. **135**(1-2): p. 132-141.
17. Murray, C.J., et al., *Global malaria mortality between 1980 and 2010: a systematic analysis*. The Lancet, 2012. **379**(9814): p. 413-431.
18. Silver, J.B., *Mosquito ecology: field sampling methods*. 2007: springer science & business media.
19. Schlyter, F., J.A. Byers, and J. Löfqvist, *Attraction to pheromone sources of different quantity, quality, and spacing: Density-regulation mechanisms in bark beetle Ips typographus*. Journal of Chemical Ecology, 1987. **13**: p. 1503-1523.

20. Kline, D.L., *Traps and trapping techniques for adult mosquito control.* Journal of the American Mosquito Control Association, 2006. **22**(3): p. 490-496.
21. Fry, R. and P. Waring, *A guide to moth traps and their use.* Vol. 24. 1996: Amateur Entomologists' Society.
22. Montgomery, G.A., et al., *Standards and best practices for monitoring and benchmarking insects.* Frontiers in Ecology and Evolution, 2021. **8**: p. 513.
23. Muirhead-Thompson, R., *Trap responses of flying insects: the influence of trap design on capture efficiency.* 2012.
24. Cannet, A., et al., *Deep learning and wing interferential patterns identify Anopheles species and discriminate amongst Gambiae complex species.* Scientific Reports, 2023. **13**(1): p. 13895.
25. Li, M., et al., *Bark beetles as lidar targets and prospects of photonic surveillance.* J Biophotonics, 2020: p. e202000420.
26. Genoud, A.P., et al., *Identification of gravid mosquitoes from changes in spectral and polarimetric backscatter cross sections.* J Biophotonics, 2019. **12**(10): p. e201900123.
27. Sugumaran, M. and H. Barek, *Critical analysis of the melanogenic pathway in insects and higher animals.* International journal of molecular sciences, 2016. **17**(10): p. 1753.
28. Berthier, S., *Iridescence.* 2007: Springer.
29. Antonelli, A. and I. Sanmartín, *Why are there so many plant species in the Neotropics?* Taxon, 2011. **60**(2): p. 403-414.
30. Eichenberg, D., et al., *Widespread decline in Central European plant diversity across six decades.* Global Change Biology, 2021. **27**(5): p. 1097-1110.
31. Nic Lughadha, E., et al., *Extinction risk and threats to plants and fungi.* Plants, People, Planet, 2020. **2**(5): p. 389-408.
32. Stohlgren, T.J., K.A. Bull, and Y. Otsuki, *Comparison of rangeland vegetation sampling techniques in the Central Grasslands.* 1998.
33. Jacquemoud, S. and S. Ustin, *Leaf optical properties.* 2019: Cambridge University Press.
34. Martinelli, F., et al., *Advanced methods of plant disease detection. A review.* Agronomy for Sustainable Development, 2015. **35**: p. 1-25.
35. Elachi, C. and J.J. Van Zyl, *Introduction to the physics and techniques of remote sensing.* 2021: John Wiley & Sons.
36. Gebru, A.K., et al. *Probing insect backscatter cross-section and melanization using kHz optical remote detection system.* in *Remote Sensing and Modeling of Ecosystems for Sustainability XIII.* 2016. SPIE.
37. Axelsson, A., et al., *Tree species classification using Sentinel-2 imagery and Bayesian inference.* International Journal of Applied Earth Observation and Geoinformation, 2021. **100**: p. 102318.
38. Synge, E., *XCI. A method of investigating the higher atmosphere.* The London, Edinburgh, and Dublin Philosophical Magazine and Journal of Science, 1930. **9**(60): p. 1014-1020.
39. Maiman, T.H., *Stimulated Optical Radiation in Ruby.* Nature, 1960. **187**(4736): p. 493-494.
40. Svanberg, S., *Atomic and molecular spectroscopy: basic aspects and practical applications.* Vol. 6. 2012: Springer Science & Business Media.
41. Brydegaard, M., A. Gebru, and S. Svanberg, *Super resolution laser radar with blinking atmospheric particles----Application to interacting flying insects.* Progress In Electromagnetics Research, 2014. **147**: p. 141-151.
42. Genoud, A.P., et al., *Insect biomass density: measurement of seasonal and daily variations using an entomological optical sensor.* Applied Physics B, 2023. **129**(2): p. 26.

43. Zhu, S., et al., *Insect abundance over Chinese rice fields in relation to environmental parameters, studied with a polarization-sensitive CW near-IR lidar system.* Applied Physics B, 2017. **123**: p. 1-11.
44. Jansson, S., et al., *Real-time dispersal of malaria vectors in rural Africa monitored with lidar.* PLoS One, 2020.
45. Brydegaard, M., *Towards quantitative optical cross sections in entomological laser radar–potential of temporal and spherical parameterizations for identifying atmospheric fauna.* PLoS One, 2015. **10**(8): p. e0135231.
46. Li, Y., et al., *Insect flight velocity measurement with a CW near-IR Scheimpflug lidar system.* Opt Express, 2020. **28**(15): p. 21891-21902.
47. Jansson, S. and M. Brydegaard, *Passive kHz lidar for the quantification of insect activity and dispersal.* Animal Biotelemetry, 2018. **6**(1): p. 1-10.
48. Kouakou, B.K., et al., *Entomological Scheimpflug lidar for estimating unique insect classes in-situ field test from Ivory Coast.* OSA Continuum, 2020. **3**(9).
49. Gebru, A., et al., *Multiband modulation spectroscopy for the determination of sex and species of mosquitoes in flight.* Journal of biophotonics, 2018. **11**(8): p. e201800014.
50. Drake, V.A. and D.R. Reynolds, *Radar entomology: observing insect flight and migration*. 2012: Cabi.
51. Chapman, J.W., D.R. Reynolds, and A.D. Smith, *Vertical-looking radar: a new tool for monitoring high-altitude insect migration.* Bioscience, 2003. **53**(5): p. 503-511.
52. Stepanian, P.M., et al., *Declines in an abundant aquatic insect, the burrowing mayfly, across major North American waterways.* Proceedings of the National Academy of Sciences, 2020. **117**(6): p. 2987-2992.
53. Long, T., et al., *Entomological radar overview: System and signal processing.* IEEE Aerospace and Electronic Systems Magazine, 2020. **35**(1): p. 20-32.
54. Behmann, J., J. Steinrücken, and L. Plümer, *Detection of early plant stress responses in hyperspectral images.* ISPRS Journal of Photogrammetry and Remote Sensing, 2014. **93**: p. 98-111.
55. Huo, L., H.J. Persson, and E. Lindberg, *Early detection of forest stress from European spruce bark beetle attack, and a new vegetation index: Normalized distance red & SWIR (NDRS).* Remote Sensing of Environment, 2021. **255**: p. 112240.
56. Lowe, A., N. Harrison, and A.P. French, *Hyperspectral image analysis techniques for the detection and classification of the early onset of plant disease and stress.* Plant methods, 2017. **13**(1): p. 80.
57. Mohammed, G.H., et al., *Remote sensing of solar-induced chlorophyll fluorescence (SIF) in vegetation: 50 years of progress.* Remote sensing of environment, 2019. **231**: p. 111177.
58. Xie, Y., Z. Sha, and M. Yu, *Remote sensing imagery in vegetation mapping: a review.* Journal of plant ecology, 2008. **1**(1): p. 9-23.
59. Kim, Y., et al., *Radar vegetation index for estimating the vegetation water content of rice and soybean.* IEEE Geoscience and Remote Sensing Letters, 2011. **9**(4): p. 564-568.
60. Calders, K., et al., *Remote sensing technology applications in forestry and REDD+*. 2020, MDPI. p. 188.
61. Axelsson, A., E. Lindberg, and H. Olsson, *Exploring multispectral ALS data for tree species classification.* Remote Sensing, 2018. **10**(2): p. 183.
62. Yu, X., et al., *Single-sensor solution to tree species classification using multispectral airborne laser scanning.* Remote Sensing, 2017. **9**(2): p. 108.
63. Bruggisser, M., et al., *Retrieval of higher order statistical moments from full-waveform LiDAR data for tree species classification.* Remote sensing of environment, 2017. **196**: p. 28-41.

64. St-Onge, B.A. and N. Achaichia, *Measuring forest canopy height using a combination of lidar and aerial photography data*. International Archives of Photogrammetry Remote Sensing and Spatial Information Sciences, 2001. **34**(3/W4): p. 131-138.
65. Lefsky, M.A., et al., *Lidar remote sensing for ecosystem studies: Lidar, an emerging remote sensing technology that directly measures the three-dimensional distribution of plant canopies, can accurately estimate vegetation structural attributes and should be of particular interest to forest, landscape, and global ecologists*. BioScience, 2002. **52**(1): p. 19-30.
66. Wulder, M.A., et al., *Lidar sampling for large-area forest characterization: A review*. Remote sensing of environment, 2012. **121**: p. 196-209.
67. Asner, G.P., et al., *A universal airborne LiDAR approach for tropical forest carbon mapping*. Oecologia, 2012. **168**(4): p. 1147-1160.
68. Meeussen, C., et al., *Structural variation of forest edges across Europe*. Forest Ecology and Management, 2020. **462**: p. 117929.
69. Lindberg, E., et al., *Estimation of 3D vegetation structure from waveform and discrete return airborne laser scanning data*. Remote Sensing of Environment, 2012. **118**: p. 151-161.
70. Ussyshkin, V. and L. Theriault, *Airborne lidar: advances in discrete return technology for 3D vegetation mapping*. Remote Sensing, 2011. **3**(3): p. 416-434.
71. Anderson, J.E., et al., *Integrating waveform lidar with hyperspectral imagery for inventory of a northern temperate forest*. Remote Sensing of Environment, 2008. **112**(4): p. 1856-1870.
72. Lindberg, E., et al., *Can airborne laser scanning (ALS) and forest estimates derived from satellite images be used to predict abundance and species richness of birds and beetles in boreal forest?* Remote Sensing, 2015. **7**(4): p. 4233-4252.
73. Davies, A.B. and G.P. Asner, *Advances in animal ecology from 3D-LiDAR ecosystem mapping*. Trends in ecology & evolution, 2014. **29**(12): p. 681-691.
74. Renfrew, C., *Prehistory: The making of the human mind*. Vol. 30. 2008: Modern library.
75. Stallman, R., *The GNU manifesto*. 1985.
76. Perens, B., *The open source definition*. Open sources: voices from the open source revolution, 1999. **1**: p. 171-188.
77. Wilczynski, V. *Academic maker spaces and engineering design*. in *2015 ASEE Annual Conference & Exposition*. 2015.
78. Pearce, J.M., *Open-source lab: how to build your own hardware and reduce research costs*. 2013: Newnes.
79. Suber, P., *Open access*. 2012: The MIT Press.
80. Adams, G.S., et al., *People systematically overlook subtractive changes*. Nature, 2021. **592**(7853): p. 258-261.
81. World Bank, *Low & middle income, Low and middle-income group aggregate. Low and middle-income economies are those in which 2022 GNI per capita was less than $13,845*. 2022.
82. Månefjord, H., et al., *BIOSPACE – A low-cost platform for problem- based learning in biophotonics*. 2021: Conference on Teaching and Learning - Proceedings, 2021. **11**.
83. Månefjord, H. *BIOSPACE Replication Files - Github repository*. 2024; Available from: https://github.com/HampusMLTH/BIOSPACE-Replication-Files.
84. Månefjord, H. *BIOSPACE code package - Github repository*. 2024; Available from: https://github.com/HampusMLTH/BIOSPACE_code_package.
85. Månefjord, H. *Hyperspecrtal lidar Acquisition LabVIEW - Github repository*. 2024; Available from: https://github.com/HampusMLTH/Hyperspecrtal-lidar-Acquisition-LabVIEW.

86. Månefjord, H. *FHSL vegetation code package - Github repository*. 2024; Available from: https://github.com/HampusMLTH/FHSL_vegetation_code_package.
87. Lindberg, D.C., *Theories of Vision from al-Kindi to Kepler*. 1976: University of Chicago Press.
88. Newton, I., *Opticks*. 1704: Dover Press.
89. Huygens, C., *Treatise on Light: In which are Explained the Causes of that which Occurs in Reflexion, & in Refraction. And Particularly in the Strange Refraction of Iceland Crystal*. 1912: MacMillan and Company, limited.
90. Young, T., *I. The Bakerian Lecture. Experiments and calculations relative to physical optics*. Philosophical transactions of the Royal Society of London, 1804(94): p. 1-16.
91. Saleh, B.E.A., et al., *Fundamentals of photonics. Pt. 1, Pt. 1*. 2019, Hoboken: Wiley.
92. Einstein, A., *On a heuristic point of view concerning the production and transformation of light*. Annalen der Physik, 1905: p. 1-18.
93. Stavenga, D.G., *Thin Film and Multilayer Optics Cause Structural Colors of Many Insects and Birds*. Materials Today: Proceedings, 2014. **1**: p. 109-121.
94. Berthier, S., E. Charron, and J. Boulenguez, *Morphological structure and optical properties of the wings of Morphidae*. Insect Science, 2006. **13**(2): p. 145-158.
95. Shevtsova, E., et al., *Stable structural color patterns displayed on transparent insect wings*. Proceedings of the National Academy of Sciences, 2011. **108**(2): p. 668-673.
96. Dou, S., et al., *Bioinspired microstructured materials for optical and thermal regulation*. Advanced Materials, 2021. **33**(6): p. 2000697.
97. Van Kooten, O. and J.F. Snel, *The use of chlorophyll fluorescence nomenclature in plant stress physiology*. Photosynthesis research, 1990. **25**(3): p. 147-150.
98. Krause, G.H. and E. Weis, *Chlorophyll fluorescence and photosynthesis: the basics*. Annual review of plant biology, 1991. **42**(1): p. 313-349.
99. Dechant, B., et al., *Canopy structure explains the relationship between photosynthesis and sun-induced chlorophyll fluorescence in crops*. Remote Sensing of Environment, 2020. **241**: p. 111733.
100. Xue, J. and B. Su, *Significant Remote Sensing Vegetation Indices: A Review of Developments and Applications*. Journal of Sensors, 2017. **2017**: p. 1353691.
101. Vogelmann, T.C., J.F. Bornman, and D.J. Yates, *Focusing of light by leaf epidermal cells*. Physiologia Plantarum, 1996. **98**(1): p. 43-56.
102. Seago, A.E., et al., *Gold bugs and beyond: a review of iridescence and structural colour mechanisms in beetles (Coleoptera)*. J R Soc Interface, 2009. **6 Suppl 2**: p. S165-84.
103. Leertouwer, H.L., B.D. Wilts, and D.G. Stavenga, *Refractive index and dispersion of butterfly chitin and bird keratin measured by polarizing interference microscopy*. Optics Express, 2011. **19**(24): p. 24061-24066.
104. Lambert, B., et al., *Monitoring the age of mosquito populations using near-infrared spectroscopy*. Scientific reports, 2018. **8**(1): p. 5274.
105. Müller, M.G., et al., *Intrinsic fluorescence spectroscopy in turbid media: disentangling effects of scattering and absorption*. Applied Optics, 2001. **40**(25): p. 4633-4646.
106. Tsien, R.Y., *The green fluorescent protein*. Annual review of biochemistry, 1998. **67**(1): p. 509-544.
107. Welch, V.L., et al. *Fluorescence in insects*. in *The Nature of Light: Light in Nature IV*. 2012. SPIE.
108. Daney de Marcillac, W., et al., *Bright green fluorescence of Asian paper wasp nests*. Journal of the Royal Society Interface, 2021. **18**(181): p. 20210418.
109. Meroni, M., et al., *Remote sensing of solar-induced chlorophyll fluorescence: Review of methods and applications*. Remote sensing of environment, 2009. **113**(10): p. 2037-2051.

110. Campbell, P.E., et al., *Contribution of chlorophyll fluorescence to the apparent vegetation reflectance.* Science of the total environment, 2008. **404**(2-3): p. 433-439.
111. Longchamps, L., et al., *Discrimination of corn, grasses and dicot weeds by their UV-induced fluorescence spectral signature.* Precision Agriculture, 2010. **11**(2): p. 181-197.
112. Mishchenko, M.I., L.D. Travis, and A.A. Lacis, *Scattering, absorption, and emission of light by small particles.* 2002: Cambridge university press.
113. Tomasi, C., et al., *Aerosol remote sensing in polar regions.* Earth-Science Reviews, 2015. **140**: p. 108-157.
114. Lee, D.W., et al., *Correlates of leaf optical properties in tropical forest sun and extreme-shade plants.* American Journal of Botany, 1990. **77**(3): p. 370-380.
115. Burresi, M., et al., *Bright-white beetle scales optimise multiple scattering of light.* Scientific reports, 2014. **4**(1): p. 1-8.
116. Yin, H., et al., *Iridescence in the neck feathers of domestic pigeons.* Phys Rev E Stat Nonlin Soft Matter Phys, 2006. **74**(5 Pt 1): p. 051916.
117. Nakamura, S., T. Mukai, and M. Senoh, *Candela-class high-brightness InGaN/AlGaN double-heterostructure blue-light-emitting diodes.* Applied Physics Letters, 1994. **64**(13): p. 1687-1689.
118. Muramoto, Y., M. Kimura, and S. Nouda, *Development and future of ultraviolet light-emitting diodes: UV-LED will replace the UV lamp.* Semiconductor Science and Technology, 2014. **29**(8): p. 084004.
119. Dissing, B.S., et al., *Using multispectral imaging for spoilage detection of pork meat.* Food and Bioprocess Technology, 2013. **6**: p. 2268-2279.
120. Hansen, K.P. and R.E. Kristiansen, *Supercontinuum generation in photonic crystal fibers.* Application Note, Crystal Fibre A/S, 2005.
121. Zhou, G., et al., *Design of supercontinuum laser hyperspectral light detection and ranging (LiDAR) (SCLaHS LiDAR).* International Journal of Remote Sensing, 2021. **42**(10): p. 3731-3755.
122. Runemark, A., et al., *Rare events in remote dark-field spectroscopy: an ecological case study of insects.* IEEE Journal of Selected Topics in Quantum Electronics, 2012. **18**(5): p. 1573-1582.
123. Hendriks, I.E., *Spectrally resolved insect flashes by sunlight*, in *Combustion physics*. 2023, Lund University.
124. Held, G., *Introduction to light emitting diode technology and applications.* 2016: CRC press.
125. Beletic, J.W., et al. *Teledyne Imaging Sensors: infrared imaging technologies for astronomy and civil space*. in *High Energy, Optical, and Infrared Detectors for Astronomy III*. 2008. SPIE.
126. Boncelet, C., *Image noise models*, in *The essential guide to image processing*. 2009, Elsevier. p. 143-167.
127. Gernsheim, H., *A concise history of photography*. 1986: Courier Corporation.
128. Ahi, K., *Mathematical Modeling of THz Point Spread Function and Simulation of THz Imaging Systems.* IEEE Transactions on Terahertz Science and Technology, 2017. **7**(6): p. 747-754.
129. Strobel, B., et al., *An automated device for the digitization and 3D modelling of insects, combining extended-depth-of-field and all-side multi-view imaging.* Zookeys, 2018(759): p. 1-27.
130. Nguyen, C.V., et al., *Capturing natural-colour 3D models of insects for species discovery and diagnostics.* PLoS One, 2014. **9**(4): p. e94346.
131. Olarte, O.E., et al., *Light-sheet microscopy: a tutorial.* Advances in Optics and Photonics, 2018. **10**(1).
132. Bernardello, M., et al., *Light-sheet fluorescence microscopy for the in vivo study of microtubule dynamics in the zebrafish embryo.* Biomedical optics express, 2021. **12**(10): p. 6237-6254.

133. Stefaniuk, M., et al., *Light-sheet microscopy imaging of a whole cleared rat brain with Thy1-GFP transgene*. Scientific reports, 2016. **6**(1): p. 28209.
134. Høye, G., T. Løke, and A. Fridman, *Method for quantifying image quality in push-broom hyperspectral cameras*. Optical Engineering, 2015. **54**(5).
135. Bianchini, V.d.J.M., et al., *Multispectral and X-ray images for characterization of Jatropha curcas L. seed quality*. Plant Methods, 2021. **17**(1): p. 1-13.
136. De La Fuente, G.N., et al., *Discrimination of haploid and diploid maize kernels via multispectral imaging*. Plant Breeding, 2017. **136**(1): p. 50-60.
137. Panagou, E.Z., et al., *Potential of multispectral imaging technology for rapid and non-destructive determination of the microbiological quality of beef filets during aerobic storage*. International journal of food microbiology, 2014. **174**: p. 1-11.
138. Brydegaard, M., et al., *Versatile multispectral microscope based on light emitting diodes*. Rev Sci Instrum, 2011. **82**(12): p. 123106.
139. Rebhan, D., et al., *Principle investigations on polarization image sensors*, in *Photonics and Education in Measurement Science 2019*. 2019.
140. Forsström, P.R., et al., *Multi-angular reflectance spectra of small single trees*. Remote Sensing of Environment, 2021. **255**: p. 112302.
141. Askoura, M.L., F. Vaudelle, and J.P. L'Huillier, *Multispectral measurement of scattering-angular light distribution in apple skin and flesh samples*. Appl Opt, 2016. **55**(32): p. 9217-9225.
142. Foschum, F. and A. Kienle, *Optimized goniometer for determination of the scattering phase function of suspended particles: simulations and measurements*. J Biomed Opt, 2013. **18**(8): p. 85002.
143. Jansson, S., et al., *First Polarimetric Investigation of Malaria Mosquitoes as Lidar Targets*. IEEE Journal of Selected Topics in Quantum Electronics, 2019. **25**(1): p. 1-8.
144. Wang, Y., et al., *International benchmarking of the individual tree detection methods for modeling 3-D canopy structure for silviculture and forest ecology using airborne laser scanning*. IEEE Transactions on Geoscience and Remote Sensing, 2016. **54**(9): p. 5011-5027.
145. Pierrottet, D., et al., *Linear FMCW laser radar for precision range and vector velocity measurements*. MRS Online Proceedings Library (OPL), 2008. **1076**: p. 1076-K04-06.
146. Brydegaard, M., et al. *The Scheimpflug lidar method*. in *Lidar Remote Sensing for Environmental Monitoring 2017*. 2017. International Society for Optics and Photonics.
147. Mei, L., et al., *Comparison studies of the Scheimpflug lidar technique and the pulsed lidar technique for atmospheric aerosol sensing*. Applied Optics, 2019. **58**(32): p. 8981-8992.
148. Carpenter, J., *Improvements in enlarging or like cameras, 1901*. British patent GB, 1901. **1139**.
149. Scheimpflug, T., *Improved method and apparatus for the systematic alteration or distortion of plane pictures and images by means of lenses and mirrors for photography and for other purposes*. GB patent, 1904. **1196**.
150. Mei, L. and M. Brydegaard, *Atmospheric aerosol monitoring by an elastic Scheimpflug lidar system*. Optics Express, 2015. **23**(24): p. A1613-A1628.
151. Liu, Z., et al., *Preliminary studies on atmospheric monitoring by employing a portable unmanned Mie-scattering Scheimpflug lidar system*. Remote Sensing, 2019. **11**(7): p. 837.
152. Mei, L., Z. Kong, and P. Guan, *Implementation of a violet Scheimpflug lidar system for atmospheric aerosol studies*. Optics Express, 2018. **26**(6): p. A260-A274.
153. Larsson, J., et al., *Atmospheric CO 2 sensing using Scheimpflug-lidar based on a 1.57-μm fiber source*. Optics Express, 2019. **27**(12): p. 17348-17358.
154. Malmqvist, E., et al., *Scheimpflug lidar for combustion diagnostics*. Optics express, 2018. **26**(12): p. 14842-14858.

155. Wang, X., et al., *Drone-based area scanning of vegetation fluorescence height profiles using a miniaturized hyperspectral lidar system.* Applied Physics B, 2018. **124**(11).
156. Malmqvist, E., *From fauna to flames: Remote sensing with scheimpflug lidar.* 2019, Lund University.
157. Brydegaard, M., et al., *High Dynamic Range in Entomological Scheimpflug Lidars.* IEEE Journal of Selected Topics in Quantum Electronics, 2021. **27**(4): p. 1-11.
158. Brydegaard, M., et al. *Short-wave infrared atmospheric Scheimpflug lidar.* in *EPJ Web of Conferences*. 2018. EDP Sciences.
159. Santos, V., et al., *Dual-Band Infrared Scheimpflug Lidar Reveals Insect Activity in a Tropical Cloud Forest.* Applied Spectroscopy, 2023. **77**(6): p. 593-602.
160. Mei, L. and P. Guan, *Development of an atmospheric polarization Scheimpflug lidar system based on a time-division multiplexing scheme.* Optics letters, 2017. **42**(18): p. 3562-3565.
161. Malmqvist, E., et al., *Effective parameterization of laser radar observations of atmospheric fauna.* IEEE Journal of Selected Topics in Quantum Electronics, 2015. **22**(3): p. 327-334.
162. Ljungholm, M., *Inelastic LIDAR for Monitoring Aquatic Fauna.* 2016.
163. Klas Rydhmer, A.S., *Applied hyperspectral LIDAR for monitoring fauna dispersal in aquatic environments.* 2016.
164. Zhao, G., et al., *Inelastic hyperspectral lidar for profiling aquatic ecosystems.* Laser & Photonics Reviews, 2016. **10**(5): p. 807-813.
165. Müller, L., et al., *Remote Nanoscopy with Infrared Elastic Hyperspectral Lidar.* Advanced Science, 2023. **10**(15): p. 2207110.
166. Salazar-Serrano, L.J., P.T. J, and A. Valencia, *A 3D Printed Toolbox for Opto-Mechanical Components.* PLoS One, 2017. **12**(1): p. e0169832.
167. Sharkey, J.P., et al., *A one-piece 3D printed flexure translation stage for open-source microscopy.* Rev Sci Instrum, 2016. **87**(2): p. 025104.
168. Zhang, X.-C., et al., *Open source 3D printers: an appropriate technology for building low cost optics labs for the developing communities*, in *14th Conference on Education and Training in Optics and Photonics: ETOP 2017*. 2017.
169. Hodgson, D. and B. Olsen, *Protecting your laser diode.* ILX Lightwave Corporation, 2003.
170. Sun, Y. and J.A. Rogers, *Semiconductor nanomaterials for flexible technologies: From photovoltaics and electronics to sensors and energy storage.* 2010: William Andrew.

Summary of Papers

Paper I (Published): A Biophotonic Platform for Quantitative Analysis in the Spatial, Spectral, Polarimetric, and Goniometric Domains

Månefjord, H., M. Li, C. Brackmann, N. Reistad, A. Runemark, J. Rota, B. Anderson, J. T. Zoueu, A. Merdasa and M. Brydegaard

This paper introduces a versatile biophotonic platform designed for optical analysis across the spatial, spectral, polarimetric, and goniometric domains. The design intricacies and calibration procedures are comprehensively detailed. Through this platform, the study demonstrated the potential to characterize varying samples such as insects, blood smears and muscle tissue. Bill of materials, assembly instructions and software needed are shared with open access.

I designed and constructed the instrument, performed calibrations and evaluations on its precision. I coded acquisition, data processing, and visualization software. I produced graphical items and wrote the manuscript.

Paper II (Published): 3D-printed Fluorescence Hyperspectral Lidar for Monitoring Tagged Insects

Månefjord, H., L. Müller, M. Li, J. Salvador, S. Blomqvist, A. Runemark, C. Kirkeby, R. Ignell, J. Bood and M. Brydegaard

This paper presents a 3D-printed hyperspectral fluorescence lidar used to remotely monitor and identify insects based on fluorescent tagging. The design considerations and calibration are detailed in the paper. The technology is demonstrated for auto-powder-tagged honeybees, and mosquitoes that consumed fluorescent-dyed sugar water. The lidar has 70 spectral bands and is the first reported measurement of remote real-time full-waveform laser-induced fluorescence spectrum during full daylight. Further due to off-the-shelf components and 3D printing it is both low cost and compact. Bill of materials, assembly instructions and software needed are shared with open access.

I designed and constructed the instrument, performed evaluations on precision. I coded acquisition, data processing, and visualization software. I conducted the study in the field, produced graphical items and wrote the manuscript.

Paper III (Published): Remote Nanoscopy with Infrared Elastic Hyperspectral Lidar

Müller, L., M. Li, H. Månefjord, J. Salvador, N. Reistad, J. Hernandez, C. Kirkeby, A. Runemark and M. Brydegaard

This paper showcases a novel hyperspectral lidar and its use in determining wing thicknesses of flying insects by analyzing their reflected wing interference patterns.

The design is derivative of that in Paper II, and I co-supervised the design process of the updated instrument. I participated in the field campaign, the coding of the acquisition software, and the writing of the manuscript.

Paper IV (In preparation): The deadliest animals with the thinnest wings – near infrared properties of tropical mosquitoes

Månefjord. H, M. Li, J. Hernandez, L. Müller, A. Merdasa, M. D. Bulo, C. Kirkeby, R. Ignell and M. Brydegaard

This paper discusses characterization of mosquitoes of different species, sex, age, and gravidity. Using short wave infrared spectroscopy, we report the thinnest insect wings in literature, and present a spectral model from which we can deduce micrometer path lengths in water and melanin.

The design is derivative of that in Paper I, and I supervised the design process of the updated instrument. I conducted the measurement, coded the acquisition software. I participated in producing the graphical items and writing the manuscript.

Paper V (In review): Hyperspectral Lidar for Monitoring High-resolution Activity Patterns of African Stingless Bee Species

Månefjord. H, A. Huzortey, R. Boateng, Y. A. Gbogbo, A. S. D. Yamoa, J. T. Zoueu, P. K. Kwapong, B. Anderson, M. Brydegaard

This paper utilizes a hyperspectral lidar for monitoring of fluorescence tagged bees. Emphasis is on the data processing and the interpretation of the results.

I organized the workshop at University of Cape Coast, Ghana, where the instrument was replicated, and the measurements taken. I conducted the data analysis, the visualization, and the writing of the manuscript.

Paper VI (In preparation): Insect Stratification & Diversity Across Taï Virgin Forest Canopy, Côte d'Ivoire – With Entomological Lidar

Månefjord. H, A. S. D Yamoa, Y. A. Gbogbo, L. Müller, A. Runemark, B. K. Kouakou, R. Boateng, A. Huzortey, I. K. Badu, M. Brydegaard, J. T. Zoueu, B. Anderson, M. Li

This paper used a kilohertz sample rate, polarization sensitive lidar, programmed to scan multiple heights inside the rainforest canopy. Resulting observations were visualized within a 3D rendering of the canopy. Hierarchical clustering was performed on the modulation spectra of the insect observations to quantify the height dependence on the insect biodiversity.

I contributed to the programming of the lidar scanning and acquisition software. I had a leading role in acquiring the field measurements. Together with Meng Li, I was responsible for visualization of the data and writing of the manuscript.

Paper VII (Published): Low-Cost and Lightweight Hyperspectral Lidar for Mapping Vegetation Fluorescence

Månefjord. H, M. Li, J. Salvador, A. Runemark, C. Kirkeby, and M. Brydegaard

This paper demonstrates the use of a hyperspectral Scheimpflug lidar for capturing vegetation fluorescence. The study remotely gathered fluorescence spectra from leaves of various native Swedish trees and constructed a three-dimensional point cloud of a forest edge. By employing dimensionality reduction and singular value decomposition, the fluorescence spectra were clustered, exploring how it can be used for classifying species.

I designed the instrument, conducted the experiment, analyzed the data, produced graphical items, and wrote the manuscript.

Paper VIII (Published): Remote Vegetation Diagnostics in Ghana with a Hyperspectral Fluorescence Lidar

Boateng. R, A. A. Huzortey, Y. A. Gbogbo, J. T. Zoueu, M. Brydegaard, B. Anderson and H. Månefjord

This paper showcases the application of the hyperspectral fluorescence lidar for remote vegetation diagnostics in Ghana. We demonstrate simultaneous remote measurements of daytime vegetation fluorescence and canopy structure. The study pinpointed the differential fluorescence responses on the upper and lower sides of leaves for stressed plants and plant species identification. The results indicate that the upper side of the leaves shows greater contrast for stress level of plants while the lower side show more deviation between species.

I organized the workshop where the instrument was replicated, and planned and directed the experiment. I supervised and project managed the process of data analysis, visualization, and writing the manuscript.

Paper IX (Published): Mapping of Algae on Walls with a 3D Printed Hyperspectral Lidar

Boateng. R, A. A. Huzortey, A. Y. Gbogbo, D. A. Yamoa, J. T. Zoueu, M. Brydegaard, H. Månefjord and B. Anderson

This paper showcases remote measurements of algae growth on buildings with a hyperspectral lidar by detecting variations in chlorophyll fluorescence.

I designed the instrument, coded the acquisition software, and organized the workshop where the instrument was replicated. The measurement was planned and executed without my involvement, but I subsequently supervised the production of graphical items and participated in the revising of the manuscript.

Paper X (Published): BIOSPACE–A low-cost platform for problem-based learning in Biophotonics

H. Månefjord, M. Li, C. Brackmann, N. Reistad, A. Merdasa and M. Brydegaard

This paper details the deployment of the Biophotonics, Imaging, Optical, Spectral, Polarimetric, Angular, and Compact Equipment (BIOSPACE) instrument in a graduate-level physics course. Its design, capabilities, and further applications are detailed in another paper. Here we focus on its pedagogical value. Since conventional biophotonic instruments are typically bulky and costly, BIOSPACE is an accessible platform for both education and research.

I designed the instrument, developed the implementation into a master course project. I produced the graphical items and wrote the manuscript.

Paper XI (Accepted): Towards Global Insect Biomonitoring with Frugal Methods

M. Brydegaard, R. D. Pedales V.Feng, A. S.-D. Yamoa, B. Kouakou, H. Månefjord, L. Wührl, C. Pylatiuk, D. de Souza Amorim, R. Meier

This paper discusses biomonitoring in low-income regions with innovative and frugal methods. Applications discussed include DNA sequencing and low-cost optical methods such as target characterization and lidar.

I designed one of the instruments discussed and produced the corresponding graphical item. I contributed to the writing of the paper.

Image attributions

[i] *Image adapted from Zephyris https://commons.wikimedia.org/wiki/File:Leaf_Tissue_Structure.svg*
[ii] *Photo by Lauro Müller*
[iii] *Illustraion adapted from Nave, Carl Rod. Hyperphysics*
http://hyperphysics.phy-astr.gsu.edu/hbase/phyopt/imgpho/polcls.png (Accessed 2024-01-08)
[iv] *Photo by Lauro Müller*
[v] *Graph by Lauro Müller, image by Meng Li*
[vi] *s-kei https://commons.wikimedia.org/wiki/File:PnJunction-LED-E.svg with CC BY-SA 2.5 DEED*
[vii] *https://imaging.teledyne-e2v.com*
[viii] *https://www.baslerweb.com*
[ix] *www.first-light-imaging.com*
[x] *Photo and drawing by Mikkel Brydegaard*
[xi] *Adapted from photo by Kendrew Schexnider*

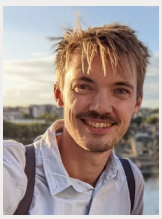

HAMPUS MÅNEFJORD works in the field of optics design and holds a master's degree in engineering physics from Lund University, Sweden. His research is featured in multiple journals focused on biophotonics, instrument design, lidar technology, and pedagogical applications. He has also presented his work on international conferences, and hosted workshops in multiple countries. This doctoral thesis explores novel instrumentation and applications in remote insect and vegetation monitoring.

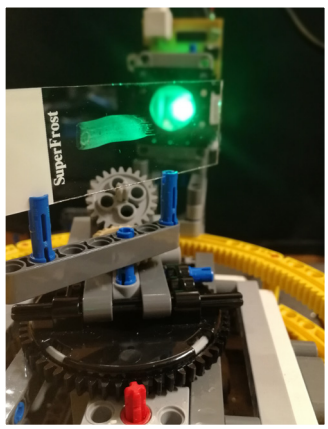

Printed by Media-Tryck, Lund 2024 NORDIC SWAN ECOLABEL 3041 0903

LUND UNIVERSITY

Department of Physics

LRCP 254
ISBN 978-91-8104-045-6
ISSN 1102-8718
ISRN LUTFD2/TCFP-254-SE